APTAMER INTERACTIONS AND APPLICATIONS IN CANCER TREATMENT

THESIS

Presented to the Graduate Council of
Texas State University-San Marcos
in Partial Fulfillment
of the Requirements

for the Degree

Master of SCIENCE

by

John R. Stecker, B.S.

San Marcos, Texas
December, 2011

APTAMER INTERACTIONS AND APPLICATIONS IN CANCER TREATMENT

Committee Members Approved:

_____
Dr. Joseph Koke, Committee Chair

_____
Dr. John Bruno, Committee Member

_____
Dr. Dana García, Committee Member

Approved:

_____
Mike Willoughby
Dean of the Graduate College

FAIR USE AND AUTHOR'S PERMISSION STATEMENT

Fair Use

Duplication Permission

ACKNOWLEDGEMENTS

First and foremost, I would like to thank my advisor Dr. Joseph Koke. From the day I first walked into his office searching for a place to begin my graduate education, he supported me where others did not. I will always be grateful to him for giving me this chance at doing something more ambitious with my life. His lessons, whether in the classroom, his office, or on the road, have all been very beneficial. Whenever I would dart into his office with a question or idea, he would stop what he was doing, listen, and give me direction. Most importantly, he kept pushing me whenever I would lose faith, not only in my work, but also in myself as a scientist. I will always be in debt to him for helping me achieve this new direction in my life.

I would also like to thank Dr. John Bruno at Operational Technologies for providing me with this project, funding, and unwavering support through all of my "trials." His quick responses and enthusiasm helped me keep pushing this project along. Dr. Bruno and Operational Technologies kept me well supplied with needed reagents, introduced me to new tools, and provided the significant financial support that kept me fed and alive to do this research. Dr. Bruno originated the concept of using aptamers to link complement proteins to these cancer cells, and I am grateful to him for entrusting me with advancing this project.

Additionally, I would like to thank Dr. Dana García for her keen insight into my work, as well as providing me with valuable advice on numerous occasions during my time

here. She helped motivate me to make sure I always thoroughly understood work that I was presenting and that those presentations were clear.

I want to acknowledge and thank Dr. Shannon Weigum for providing me with an extremely valuable crash course in ImageJ and cell image analysis. The majority of results and the cool looking figures in this paper are a direct result of her help.

I would like to thank Alissa Savage for the huge amount of work she put into the TEM imaging used in this project, teaching me a great deal about TEM imaging, and the critical role she played in working through the methods for getting these samples in a state that could be imaged. Her driving work ethic was an inspiration, especially when things were tough. I also owe a great deal to Mya Patel for teaching me the science of culturing cells. She helped me settle into the lab, and her no nonsense attitude really helped to keep me on target with all of my work. I want to also thank my lab-mate Luis Neve for acting as a soundboard for so many of my ideas, for his thoughts, and for the numerous energy drink fueled all-night study sessions. I want to additionally thank my lab mates Sarah Kane and Andrew Weems, both of whom helped to keep my cells alive when I had to be out, in addition to all the great brainstorming and insight.

Finally, I want to thank my wife Erin Stecker, who supported me throughout this endeavor; so much so that she was willing to marry me half-way through. I could not have accomplished this with out her.

This work has been supported by funding from OTC Biotechnologies, LLC, the Biology Department of Texas State University, the Texas State Vice President for Research and Federal Affairs, and the National Science Foundation (DBI-0821252).

This manuscript was submitted on 08/09/2011.

TABLE OF CONTENTS

Page

LIST OF TABLES

Table **Page**

LIST OF FIGURES

Figure **Page**

ABBREVIATIONS USED

Ab - Antibody
AF546 – AlexaFluor 546
ATCC – American Type Culture Collection
DMEM – Dulbecco's Modified Eagle's Medium
Dox – Doxorubicin
EMS - Electron Microscopy Sciences
EtOH - Ethanol
FBS – Fetal Bovine Serum
FRET – Förester Resonance Energy Transfer
HSCP – Human Serum Complement Proteins
IDT - Integrated DNA Technologies
LSCM – Laser Scanning Confocal Microscopy
MAC – Membrane Attack Complex
mCRPs – Membrane Complement Regulatory Proteins
MEAR - BNL 1ME A.7R.1 cell line
OpTech – Operational Technologies Corp., San Antonio, TX
PBS – Phosphate Buffer Saline
PSMA – Prostate-Specific Membrane Antigen
ROI – Region of Interest
RT – Room Temperature (approx. 25°C)
SAv – Streptavidin
SELEX - Systematic Evolution of Ligands by EXponential enrichment
SEM – Scanning Electron Microscopy
TEM – Transmission Electron Microscopy

ABSTRACT

APTAMERS AND THEIR USE IN CANCER TREATMENT VIA THE HUMAN COMPLEMENT PATHWAY

by

John Richard Stecker, B.S.

Texas State University-San Marcos

December 2011

SUPERVISING PROFESSOR: Joseph R. Koke

Aptamers, small strands of RNA or DNA, are finding a rapidly expanding repertoire of applications. Aptamers have found numerous diagnostic and therapeutic uses both *in vitro* and *in vivo*. Specifically, their application in diagnosis and treatment of multiple cancers has been strongly advanced over the last decade. In this study, two different applications of aptamers are explored for two different cancers. In the murine liver cancer cell line, BNL 1ME A.7R.1 (MEAR), the TLS-11a aptamer is shown to quickly internalize at physiological temperatures. The TLS-11a aptamer is therefore a potential candidate for intracellular toxin delivery as a means of inducing targeted apoptosis of the MEAR cancer cells. In the human

breast cancer cell line MCF7, the MUC1-5TR aptamer is shown to successfully initiate the classical complement pathway leading to complement fixation on the target cell via a streptavidin-C1q conjugation. This model provides a way to help the human immune system specifically target and remove cancerous cells.

CHAPTER 1

INTRODUCTION

According to the website for the National Cancer Institute (NCI), a member of the U.S. National Institutes of Health, just over 1.5 million people were diagnosed with cancer in 2010, and over half a million people died that year from it. In the NCI's recent publication, "Cancer : Changing the Conversation," they list their 2012 budget request at almost $6 billion. However, this is minor in comparison with the National Institutes of Health estimates for total overall costs; in 2008, this was estimated at around $228.1 billion (American Cancer Society, 2009).

A promising development is the use of artificial short biological constructs, termed "aptamers", made from DNA, RNA, or amino acids. By folding into specific tertiary structures, aptamers can act as surrogates for antibodies by forming highly stable complexes with selected targets (Ellington and Szostak, 1990; Ferreira et al., 2006, 2008; Shangguan et al., 2008). Aptamers also appear to be significantly less immunogenic as compared to non-self antibodies, making them highly preferable to traditional antibiotic or monoclonal antibody based therapeutics (Osborne et al., 1997).

Aptamers are already used in the detection, diagnosis, and treatment of many diseases. The best example of a therapeutic application of an aptamer is the FDA approved drug pegaptanib, brand name Macugen®, developed by Gilead Sciences for the treatment of age-related macular degeneration (Zhou and Wang, 2006). The aptamer is injected into the affected eye where it binds to, and inhibits, the vascular endothelial growth factor isoform

$VEGF_{165}$ (Waheed and Miller, 2004). VEGF is a major growth factor in angiogenesis (Malik and Gerber, 2003) and is thought to be responsible for the abnormal growth of blood vessels causing the more severe form of the disease (Berdeaux et al., 2005). Overexpression of VEGF in cancer has also made it a highly desired target for aptamer-based cancer therapy (Malik and Gerber, 2003). Aptamers have successfully been used to inhibit $VEGF_{165}$ (Huang et al., 2001) and other proteins in the angiogenesis signaling pathways in tumors (Sarraf-Yazdi et al., 2008) as a means to inhibit tumor growth both *in vitro* and *in vivo*. In addition to inhibiting VEGF, anti-VEGF aptamers have been immobilized on materials such as silicon nanowires (Lee et al., 2009) and nanotubes (Kwon et al., 2010) to create biosensors. The binding of VEGF to the anti-VEGF aptamers causes a change in conductance in field effect transistors on the biosensor. This change can be detected and translated into a concentration of VEGF, potentially leading to earlier and better cancer detection systems.

Aptamers are also being used as a synthetic, targeted delivery system by conjugating them to the desired "cargo" (Lee et al., 2010). Aptamers selected for proteins that are over-expressed in cancerous cells have been used to successfully deliver the DNA crosslinking drug cisplatin to MCF7 breast cancer cells via liposomes (Cao et al., 2009) and LNCaP prostate cancer cells via controlled release nanoparticles (Dhar et al., 2008). Doxorubicin (dox), a cancer chemotherapeutic drug that intercalates DNA to halt replication by inhibition of topoisomerase, has also been loaded directly into an aptamer targeting prostate-specific membrane antigen (PSMA) on LNCaP prostate cancer cells (Lee et al., 2011), reducing both cell viability and inhibiting tumor growth. Another group developed a dual dox loaded aptamer system targeting both PSMA(+) and PSMA(-) prostate cancer cells via a streptavidin conjugate (Min et al., 2011). Cell viability was reduced to a level equivalent to treating the

cells directly with dox. In cell lines that did not express PSMA(+) or PSMA(-), the cell viability was almost completely unaffected by the dox-aptamer bioconjugate, meaning that the conjugation of dox with the aptamers actually inhibits the toxic effects of dox towards any cell that is not the target cell.

Relevant to this research, the first protein in the human classical immune pathway of complement activation has been conjugated to an aptamer specific for the mucin 1 glycoprotein expressed on MCF7 breast cancer cells, via a biotin-streptavidin linker, which resulted in complement-mediated lysis of the cancer cells (Bruno, 2010). See Figure 1 for an example. He was also successful with this approach using an aptamer designed against lipopolysaccharide from *E. coli* (Bruno et al., 2008).

The classical pathway of complement activation is one of three protein cascades that the immune system uses to initiate formation of membrane attack complexes (MACs) into the membrane of an invading pathogen or cell. Reviewed thoroughly by Eric Wagner and Michael M. Frank (Wagner and Frank, 2010), the classical pathway begins with the binding (typically to an appropriate immunoglobulin) of, and activation of, the complement protein C1qrs. Activation of C1qrs gives it the ability to cleave C4 and C2 into smaller (a and b) fragments. C4a and C2b bind together and to the surface of the target cell to form the classical C3 convertase, C4aC2b.

The classical C3 convertase then cleaves the C3 protein into two component parts, also designated a and b. Interaction of the classical C3 convertase with the C3b component is called the C5 convertase. This enzyme is able to cleave C5 into C5a and C5b. C5b binds to the surface of the cell and recruits C6 and C7. This binding event is the beginning of the MAC formation. These three proteins are able to recruit C8, which embeds into the membrane and recruits multiple C9 proteins until the pore is formed, at which point the

MAC is complete. The continued embedding of MACs into the cell membrane destroys the integrity of the cell membrane resulting in osmotic lysis. See Figure 1 for a summary of this pathway, as well as the aptamer-SAv-C1qrs complex.

There are a number of membrane-bound complement regulatory proteins (mCRPs) that function to keep the various complement pathways from acting unchecked and destroying healthy cells. The expression of these regulatory proteins across a large number of cancers has been thoroughly reviewed (Fishelson et al., 2003). The mCRP CD59 is highly expressed in human breast cancers and functions by binding to C8 and C9 proteins (Thorsteinsson et al., 1998), preventing C9 from binding to the C5b-8 complex (Qian et al., 2000), and inhibiting MAC formation. In order for complement-mediated lysis of cells to occur, the cascade must overcome these proteins once fixation to the cell surface has begun.

Success in overcoming the inhibitory effects of mCRPs in complement-mediated lysis studies has been investigated through the use of antibodies (Ab) that bind to and inhibit specific mCRPs. Inhibiting CD59 via a specific monoclonal antibody and exposure to complement serum was sufficient to significantly increase the lysis of T47D breast carcinoma tumor spheroids (Hakulinen and Meri, 1998). Antibody-mediated complement activation and cell lysis has also been augmented by the specific inhibition of the mCRPs CD46, CD55, and CD59, having the greatest effect when inhibited in concert with each other (Jurianz et al., 1999).

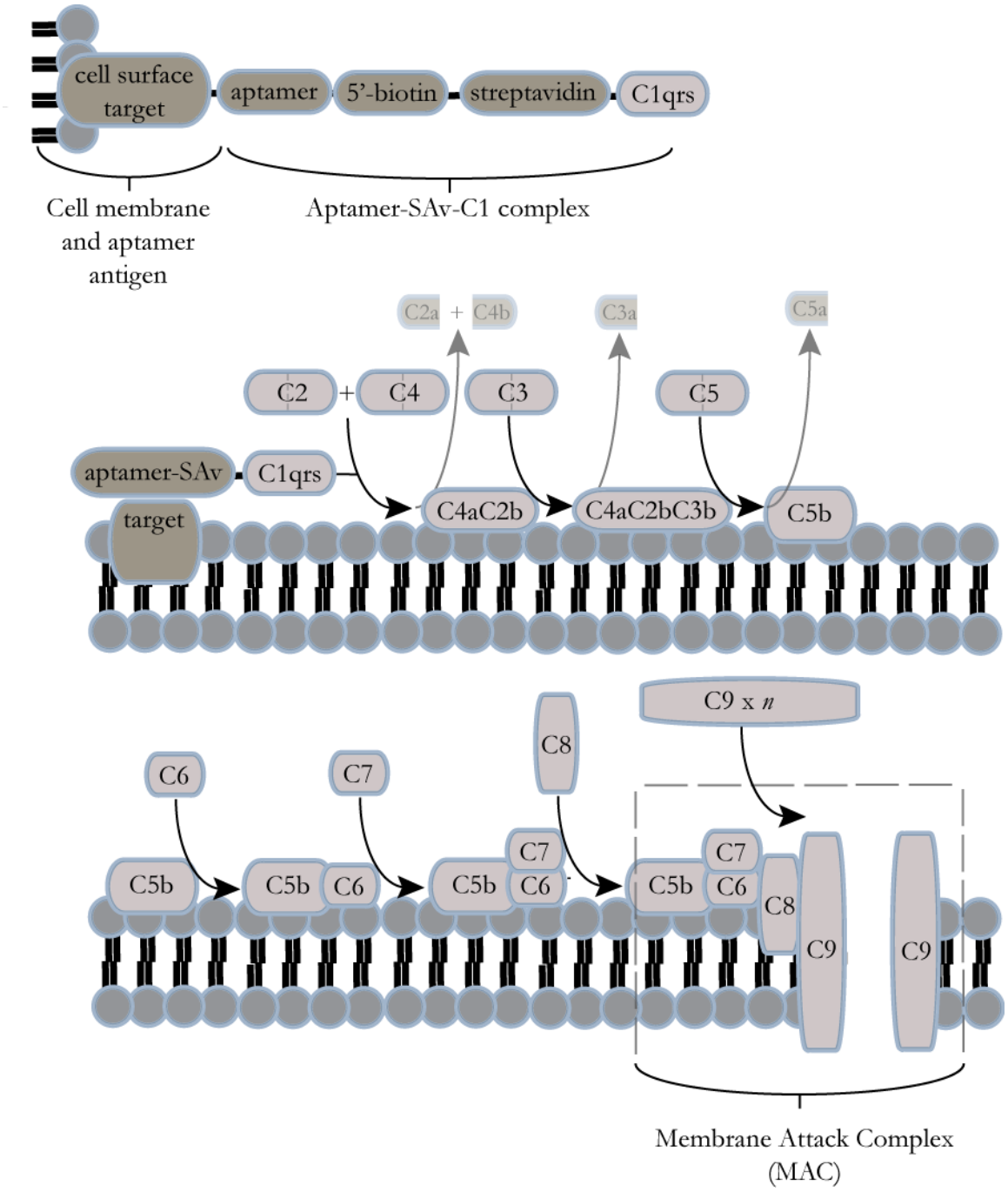

Figure 1. Aptamer-SAv-C1qrs Complex and Classical Complement Cascade.

This study tested the hypothesis that DNA aptamers, coupled with elements of the complement pathway, could specifically attach to cancer cells, and in the presence of human complement serum, catalyze the formation of the membrane attack complex (MAC), and cause lysis and death of the cells. Dr. John Bruno has previously tested this hypothesis with the MCF7 breast cancer cell line via quantification of Trypan blue absorbance, a method for labeling dead or dying cells, as well as some immunofluorescence staining for aptamer-biotin-SAv-C1q and C9 deposition (Bruno, 2010). The present study sought to expand upon his investigation in a number of ways. The binding kinetics of aptamers and SAv-C1q was analyzed. An expanded analysis of C9 deposition through immunocytochemistry including the effects of the MAC-inhibiting membrane complement regulatory protein (mCRP) CD59 was conducted. The kinetics of MAC formation using Förster resonance energy transfer (FRET) was investigated, as well as a morphological investigation using transmission electron microscopy (TEM).

Two specific cell lines were chosen to test this hypothesis; a human breast adenocarcinoma cell line called MCF7 and a murine liver tumorigenic cell line called BNL 1ME A.7R.1, or MEAR. Two aptamers, one for each cell line were selected on the basis of previously published results. The MUC1-5TR aptamer was selected for the MCF7 cell line (Ferreira et al., 2008), and binds to mucin 1 (MUC1), a proteoglycan that is heavily overexpressed in breast cancers (Mukhopadhyay et al., 2011). The TLS-11 aptamer was selected for the MEAR cell line (Shangguan et al. 2008). The surface target it binds to is currently unknown (Table 1).

Table 1. Aptamer Information Summary

Aptamer	Cell Line	Sequence	K_d (nM)	Reference
MUC1-5TR	MCF7	5′-GGGAGACAAG AATAAACGCT CAAGAAGTGA AAATGACAGA ACACAACATT CGACAGGAGG CTCACAACAG GC-3′	47.3	Ferreira et al. 2008
TLS-11a	MEAR	5′-ACAGCATCCC CATGTGAACA ATCGCATTGT GATTGTTACG GTTTCCGCCT CATGGACGTG CTG-3′	4.51 +/- 0.39	Shangguan et al. 2008

CHAPTER 2

MATERIALS AND METHODS

Experimental Design

The high specificity of aptamers was exploited by conjugating a biotin linker to the 5' end of the aptamer, performed by the vendor Integrated DNA Technologies (IDT), then conjugating the first protein of the immune system's classical complement pathway, C1q, to streptavidin, which has four highly specific binding sites for biotin. In this way, the immune system can be directed towards the target cell. The intent was to cause complement fixation on the target cell, formation of the membrane attack complex (MAC) on its surface, and lysis of the cell resulting in cell destruction. Intermediate steps in this design employed aptamers-biotin-streptavidin bioconjugates linked to various fluorophores to enable better visualization binding dynamics and post-binding events using laser-scanning confocal microscopy (LSCM) and transmission electron microscopy (TEM).

Laser Scanning Confocal Microscopy

LSCM was performed using an Olympus FV1000 system (Olympus America - http://www.olympusamerica.com/seg_section/product.asp?product=1008). Details of image acquisition are presented in the figure legends. Primary processing of images including quantitation of fluorescence intensity was performed using the Olympus FV1000 software and post-processing for publication used Adobe Photoshop CS

(http://www.adobe.com) and the National Institute of Health's open source software ImageJ (rsbweb.nih.gov/ij/).

Cell Culture

BNL 1ME A.7R.1 (MEAR) and MCF7 cells obtained from American Type Culture Collection, Manassas, VA (www.atcc.org), were used as model cancer cells for this study. MEAR cells are a chemically transformed tumorigenic liver cell line from the BALB/c strain of *Mus musculus* (mouse). MCF7 cell cultures are a human female breast adenocarcinoma-derived cell line. For the control cell line in the Aptamer Binding Specificity portion of this study, F98 cell cultures were also obtained from ATCC. F98 cells are an undifferentiated malignant glioma cell line derived from *Rattus norvegicus* (rat) brain.

Culture reagents were supplied either by ATCC or Sigma Aldrich, St. Louis, MO (http://www.sigmaaldrich.com/). MEAR cells were cultured in a 1:1 mix of Dulbecco's Modified Eagle's Medium (DMEM) and Ham's F-12 Medium with 0.5% insulin-transferrin-selenium for a final concentrations of 5 μg/ml, 2.75 μg/ml, and 0.1 μg/ml respectively. The medium was additionally supplemented with 1% penicillin-streptomycin, 10% heat-inactivated fetal bovine serum (FBS), and 0.1mg/l epidermal growth factor. MCF7 cells were cultured in RPMI-1640 supplemented with 10% FBS and .1% Bovine Insulin (Sigma Aldrich). F98 cells were cultured in DMEM supplemented with 10% FBS. Cells were incubated at 37°C in a 95% air, 5% CO_2 humid atmosphere. Sub-culturing was done when cell confluence reached approximately 90%, and was typically sub-cultured at a 1:3 flask ratio. Trypsin/EDTA (ATCC) was used to detach adherent cells, which were centrifuged at approximately 274 xg for 5 minutes before sub-culturing.

Aptamer Synthesis and Binding Kinetics

Aptamers were synthesized with various modifications by Integrated DNA Technologies, Coralville, Iowa (http://www.idtdna.com). See Table 1 for sequence, binding affinity, and reference information. Both aptamers were developed utilizing the SELEX (Systematic Evolution of Ligands by EXponential enrichment) process (Tuerk and Gold, 1990). The SELEX process utilizes multiple rounds of binding, washing, detaching, and replicating a library of random sequence oligonucleotides that eventually results in a small number of aptamers with a high binding affinity for the target (Ellington and Szostak, 1990, Tuerk and Gold, 1990). This process typically results in >90% of the enriched library binding to the target (Jayasena, 1999). Aptamer secondary structure was predicted using the Vienna RNA secondary structure server (Hofacker, 2003) at http://rna.tbi.univie.ac.at/cgi-bin/RNAfold.cgi, selecting the DNA energy parameters and desired temperatures. Free energy minimization is used to calculate the 2° stem-loop structures. Predicted structures were compared to those predicted by Integrated DNA Technologies (IDT) folding program UNAFold, at http://www.idtdna.com/Scitools/Applications/unafold/ to corroborate structure (results not shown).

Aptamer binding specificity was determined by conjugating MUC1-5TR and TLS-11a aptamers to AlexaFluor-546 (IDT) and adding 200 µl of 1.5 mg/ml in either binding buffer (0.5 M NaCl, 10 mM Tris-HCl, and 1 mM $MgCl_2$, in nuclease free H_20, pH 7.5-7.6; Bruno, 2010), for the MUC1-5TR aptamer, or phosphate buffer saline (PBS) for the TLS-11a aptamer, to live cultures (80% or more confluent) of MEAR cells and MCF7 cells, as well as F98 cells as a negative control. Cells were imaged via LSCM 5 minutes after treatment.

Binding kinetics were determined by adding 200 µl of 1.5 mg/ml TLS-11a-AF546 to MEAR cells while continuously imaging by LSCM. Imaging began 15 minutes prior to addition of the aptamer conjugate and continued 30 minutes following for a total of 45 minutes, and was performed both at 25°C and 37°C. For imaging at 37°C, cells were first grown on 18 mm circular coverslips. Before aptamer treatment, they were transferred to a special heated-stage dish designed for the Bioptechs heated-stage system using the Delta T5 System controller, as seen in Figure 2.

After surface binding, the TLS-11a aptamer streptavidin AlexaFluor-546 conjugate unexpectedly was rapidly internalized by MEAR cells in a temperature-dependent fashion. Internalization of the MUC1-5TR aptamer after binding to the cell surface of MCF7 cells did not occur. For imaging, cells were treated with 100 µl of 1.5 mg/ml TLS-11a aptamer streptavidin AlexaFluor-546 conjugate for approximately 5 minutes, then imaged as described above at 25°C and 37°C. Images were taken continuously over 45 minutes to create a video of the aptamer movement into the cells.

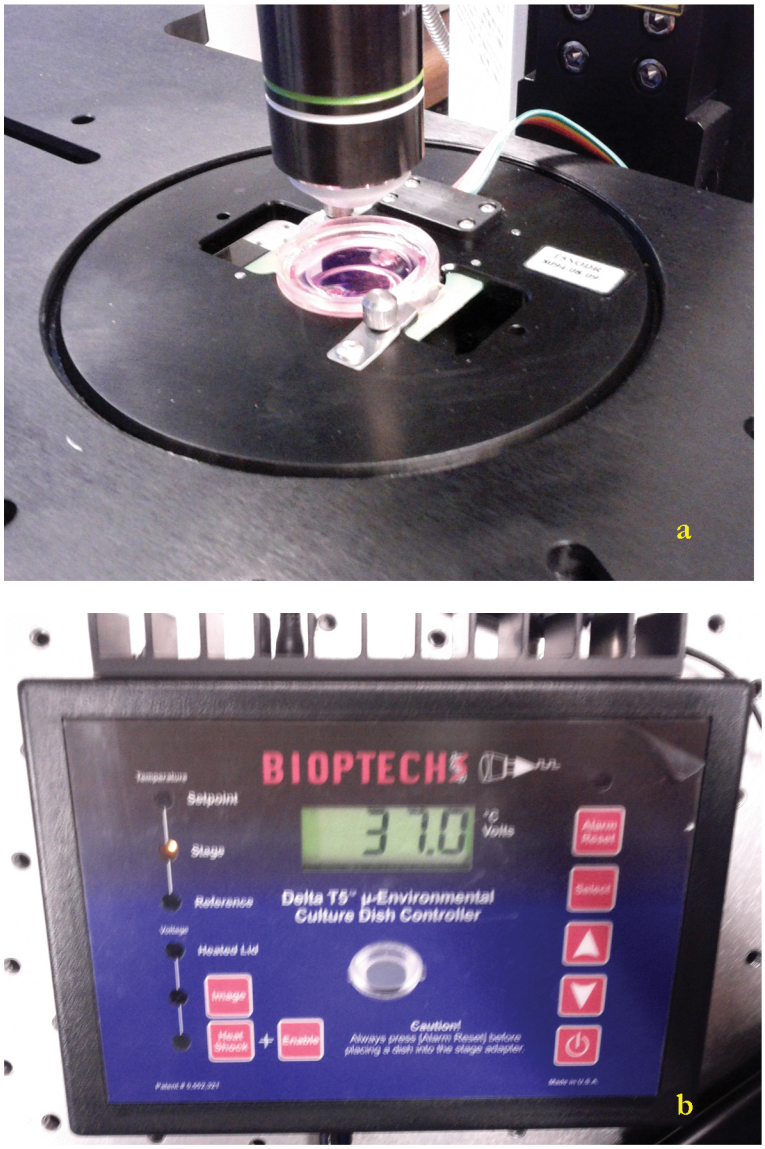

Figure 2. Bioptechs Heated Stage System. Image *(a)* shows the culture dish hooked into the heated stage. Image *(b)* shows the controlling system.

Complement Treatment

To initiate MAC formation due to complement activation, MCF7 cells were first washed twice in 3 ml of binding buffer for 5 minutes to remove any shed or loose MUC1. This step was unnecessary for the MEAR cell line. Following this, 2.4 ml of fresh media was then added back to the cell dishes, followed by 200 µl of the appropriate 5'-biotinylated aptamer at a concentration of 1.5 mg/ml for 5 minutes. 200 µl of Streptavidin-C1q conjugate (SAv-C1q) was added for 10 minutes, followed by 200 µl Human Serum Complement Proteins (HSCP) 3 hours (Bruno, 2010). For inhibition of the mCRP CD59, the monoclonal rat anti-human CD59 antibody YTH53.1 (LifeSpan BioSciences, Inc., Seattle, WA) was used at a 1:4 dilution.

Immunocytochemistry

MEAR and MCF7 cells were grown on square coverslips in culture dishes to an 80-90% confluent layer. Each cell line was incubated with the appropriate aptamer (Table 2). The cells were then washed twice in binding buffer for 5 minutes each and then fixed in methanol for 1 minute. After drying, the cells were washed 3 times in binding buffer for 10 minutes per wash, then blocked with 20% non-fat dry milk for 2 hours at room temperature. After 3 more binding buffer washes at 10 minutes per wash, the cells were incubated in 1:20 monoclonal mouse anti-human C9 antibody (United States Biological, Swampscott, MA) overnight at 4°C.

After three 10 minute binding buffer washes, cells were blocked with 20% non-fat dry milk for 2 hours, followed by another three 10 minute PBS washes. The cells were then incubated with a 1:300 anti-mouse secondary antibody conjugated to Cy5 (Invitrogen) for 2

hours at room temperature. Cells were again washed three times in binding buffer for 10 minutes per wash, incubated for 20 minutes with a 1:2000 Hoechst nuclear stain, washed again, mounted in glycerol and viewed on a single-photon LSCM system.

Förster Resonance Energy Transfer Analysis

The voltage sensitive probes dimyristoylphosphatidylethanolamine (CC2-DMPE) as the donor and bis-(1,3-diethylthiobarbituric acid)trimethine oxonol ($DiSBAC_2(3)$) as the acceptor were used to signal membrane depolarization due to MAC formation. Both probes were provided as a kit from Invitrogen, Carlsbad, CA (www.invitrogen.com). The CC2-DMPE donor was loaded at a concentration of ~ 10 μM for 30 minutes in the dark at RT and, after a brief wash in medium, the $DiSBAC_2(3)$ acceptor was loaded at 10 μM, along with 250 μl aptamer (1.5 mg/ml) and 200 μl SAv-C1 conjugate or 450 μl binding buffer as a control.

A single 405 nm laser was used to excite the loaded MCF7 cells. The cells were then scanned over time via LSCM. While scanning, 200 μl HSCP was added to both groups. Pre- and post-HSCP images were then analyzed using the ImageJ software, and emission and response ratios were calculated in Microsoft Excel. See Appendix E for raw data.

Transmission Electron Microscopy

TEM imaging was used to search for MACs and to statistically analyze differences in cell swelling and MAC formation between treatment and control groups. The swelling was expected due to the osmotic movement of water into the cell due resulting from MAC formation. The cells were detached from their dishes using Typsin/EDTA, then pelleted at 274 xg for 5 min. Cells were resuspended in 3 ml of MEM. The experimental group was

treated with 250 µl of biotinylated MUC1-5TR aptamer for 5 minutes, then 200 µl of SAv-C1 and 200 µl of HSCP for 3 hours. The negative control was treated with equal volumes of binding buffer, and the complement control received 450 µl of binding buffer and 200 µl of HSCP.

Cells were then pelleted in 3% glutaraldehyde fixative in 0.05 M cacodylate buffer, pH 7.5 and fixed overnight at 4°C. Cells were washed 3 times at 15 minutes each in .05 M cacodylate buffer by re-pelleting, without resuspension. Cells were then fixed with 1% OsO_4 in 0.1 M cacodylate buffer, pH 7.5 for 3 hours. Cells were then washed in binding buffer again, twice at 15 minutes, and once more overnight. Following this, the cells were dehydrated with two 30 minute washes of 70% ethanol (EtOH). Pellets were embedded in London Resin White (Electron Microscopy Supplies, For Washington, PA) and 70% EtOH (2:1 mixture) for 1 hour, then three 30 minute washes in 100% LR White followed by 48 hours at 60°C for polymerization.

Samples were cut into 70 nm sections using a Leica Reichert Ultracut S ultramicrotome with a diamond knife, and collected on 200 hex nickel grids. Imaging was done on a JEM-1200EX II TEM system. Images were captured by a Gatan SC1000 ORIUS® CCD TEM digital camera. Image editing was done using Gatans' Digital Micrograph™ and Adobe Photoshop 12.0.

To avoid bias in image acquisition and statistical analysis, a double-blind experiment was set up by re-labeling groups for image acquisition, and re-labeled again for analysis of the data. Care was taken to avoid counting a cell twice. A standard area was determined to use for cell counting across all grids, and only cells with a visible nucleus were counted. To determine if the cell was swollen, low magnification images (7500, 10K, or 12K) were used.

If there was any ambiguity in determining if a cell was swollen, the cell would be counted as not swollen. A single 200K image was taken of the membrane at 0°, 90°, 180°, and 270° from the nucleus to check for membrane breaks. 20 cells from each group were analyzed.

Data were analyzed using the open-source R stats software from http://www.r-project.org (Hornik, 2011). Associations between membrane breaks and swollen cells were determined by calculating odds differences by hand, and the Fisher's Exact Test. Differences in the proportions of swollen cells was determined using the R Test of Equal or Given Proportions (see Appendix F).

CHAPTER 3: RESULTS

Aptamer Secondary Structure Prediction

The MUC1-5TR 2° aptamer structure, using free energy minimization, was predicted for 37°C and 25°C as all experiments were conducted at those two temperatures, and because the aptamer was originally selected at 37°C. The TLS-11a aptamer structure was predicted at both 37°C and 25°C and additionally at 4°C as this aptamer was originally selected on ice. Figure 3 shows the results of the structure prediction for the MUC1-5TR aptamer, and Figure 4 shows the TLS-11a aptamer.

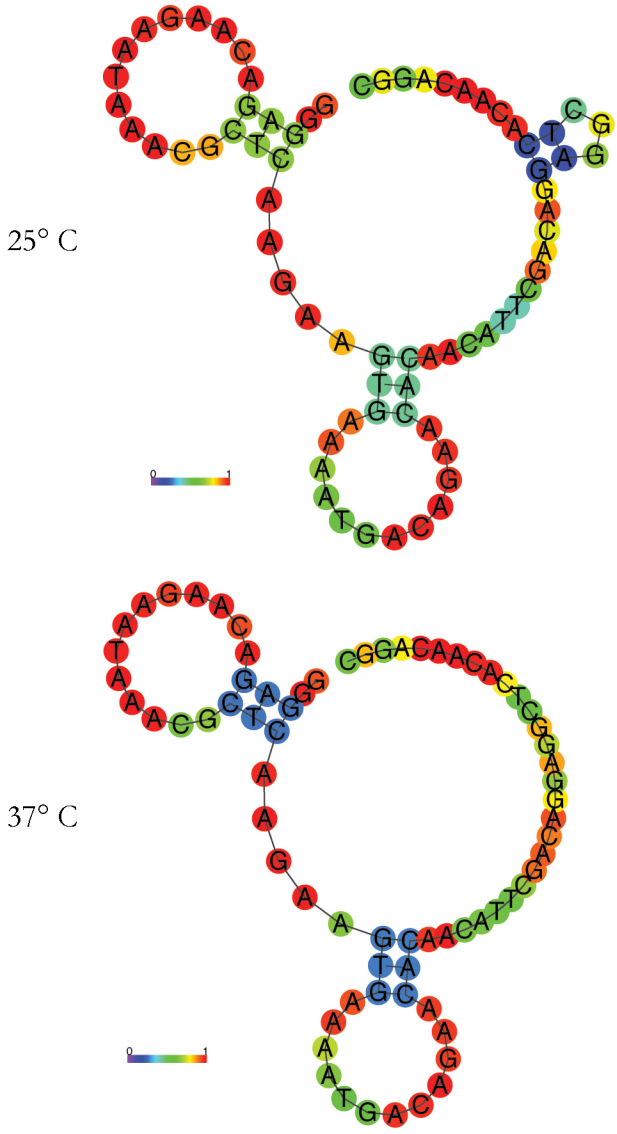

Figure 3. MUC1-5TR Predicted Structures. MUC1-5TR predicted stem-loop structures via the Vienna RNA secondary structure server; using DNA parameters and free energy minimization. Color scale represents base pair location probabilities.

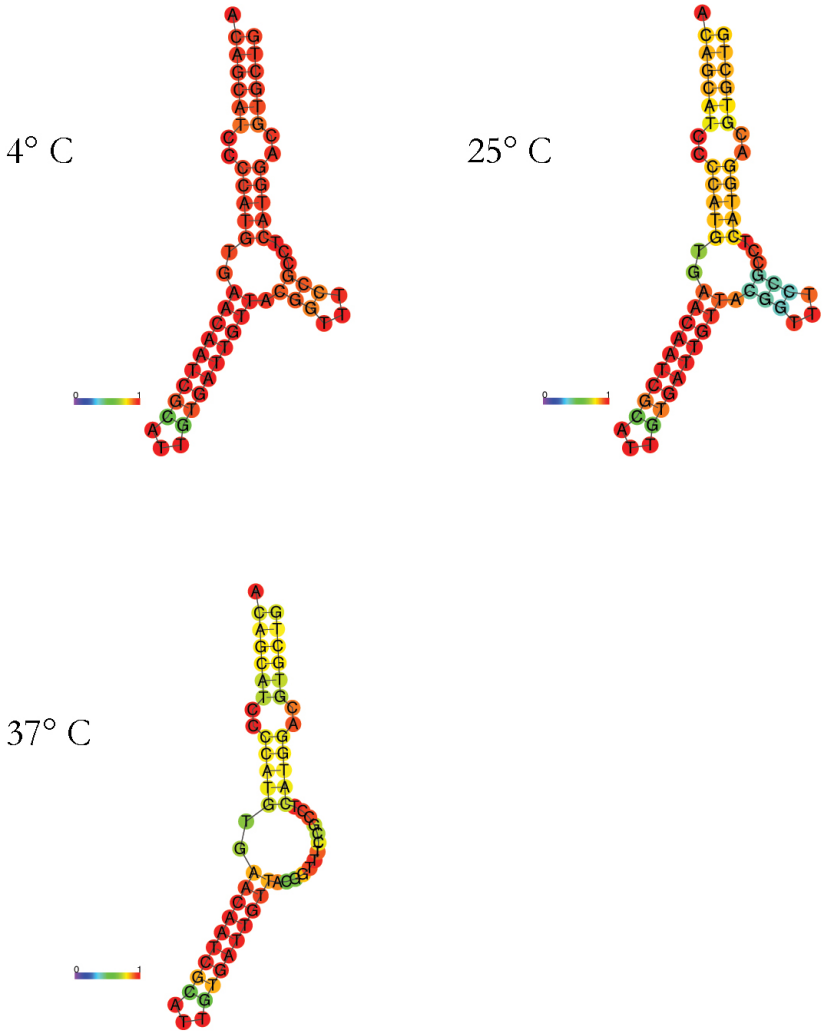

Figure 4. TLS-11a Predicted Structures. TLS-11a predicted stem-loop structures via the Vienna RNA secondary structure server; using DNA parameters and free energy minimization. Color scales represent base pair location probabilities.

Aptamer Binding

The TLS-11a-AF546 aptamer bound to the MEAR cells produced bright fluorescent labeling. Little to no fluorescence was visible when MEAR cells were treated with the MUC1-5TR-AF546 aptamer, a test to ensure that AF546 itself is not binding to the cell. Conversely, the MUC1-5TR-AF546 aptamer bound to the MCF7 cells produced bright fluorescent labeling, but little to no visible fluorescence when treated with the TLS-11a-AF546 aptamer. The F98 cells were not decorated by either aptamer (Figure 5).

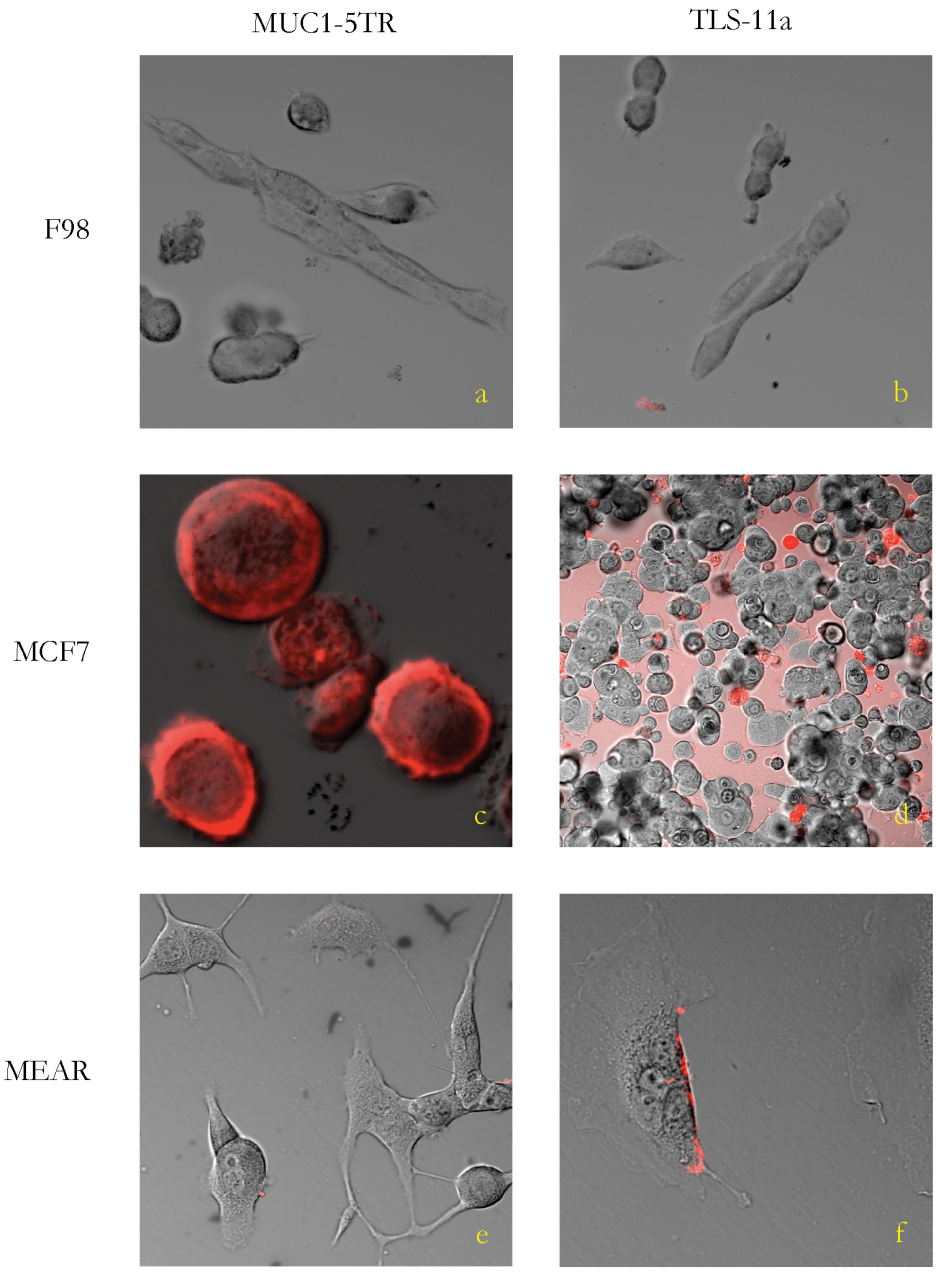

Figure 5. Aptamer Binding Matrix. F98 (*a* and *b*), MCF7 (*c* and *d*), and MEAR (*e* and *f*) cells exposed to either the MUC1-5TR aptamer (left column) or the TLS-11a aptamer (right column). Fluorescence in *d* is either background or aptamer sticking to cell debris.

Aptamer Binding Times

Addition of TLS-11a aptamers conjugated to AF546 decorated the cell membrane of MEAR cells within 5 minutes of treatment, as seen in Figure 6, image *a*. A cell was chosen from the field of view and three regions of interest (ROIs) on that cell were chosen to analyze. The average pixel intensity value for each ROI was determined for various time points and then graphed. The aptamer-AF546 was added at about 150 seconds into the scan, and rose to an easily detectable level within 3 to 5 minutes.

SAv-AF546 was added to cells that had been treated with biotinylated aptamer 5 minutes prior. A cell was isolated from the scan, as seen in Figure 6, image *b*, and three ROIs were chosen for analysis. By plotting the average pixel intensity value for each ROI over time, it was determined that maximal fluorescence was reached in just under 3 minutes from addition.

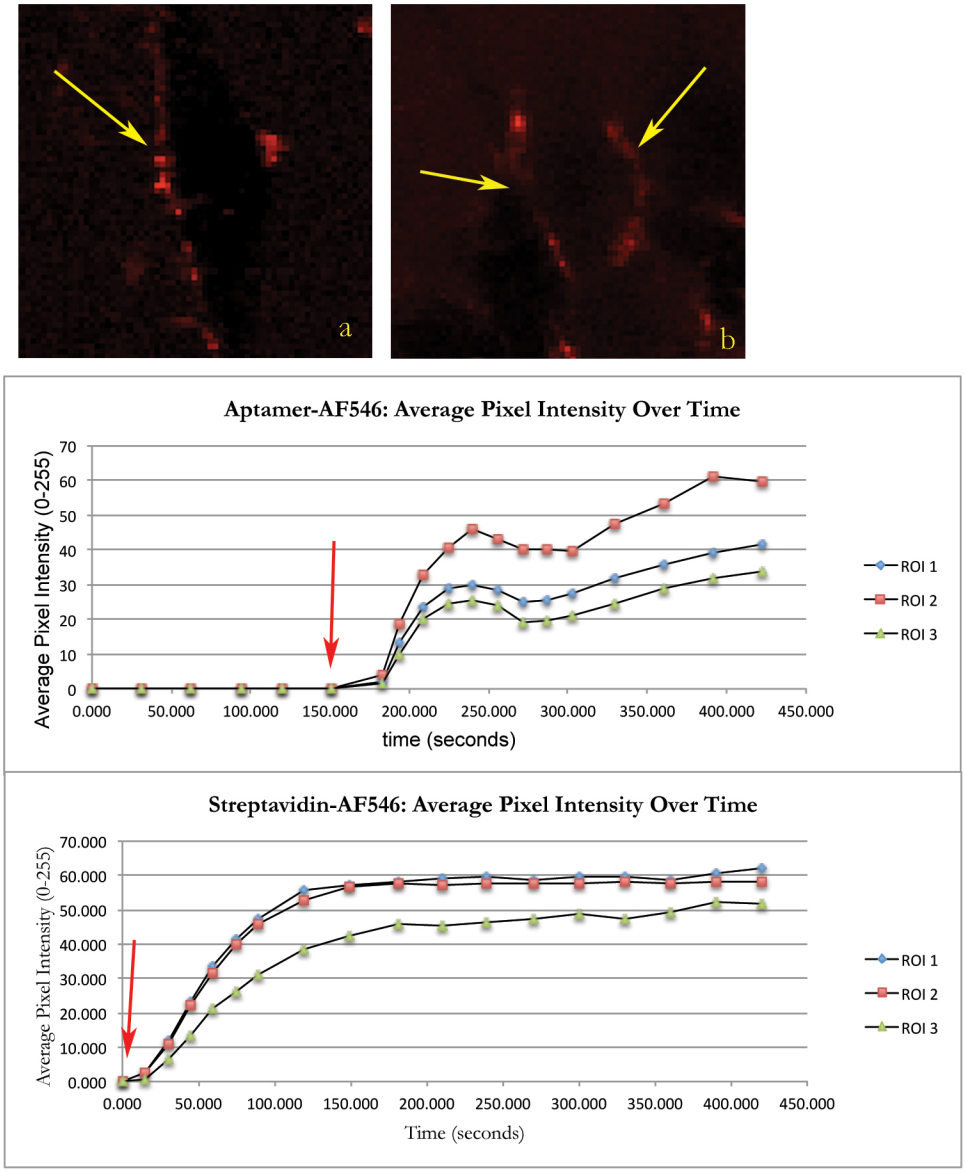

Figure 6. Aptamer/SAv Binding Dynamics. LSCM was used to capture over time increasing fluorescence of aptamer-AF546 *(a)* or SAv-AF546 (*b*). Yellow arrows indicate membrane labeling. A single cell was chosen in each experiment, and three ROIs were identified on each cell. The change in the average pixel intensity value (0 – 255) was measured and graphed over time. Red arrows indicate the point during imaging that the treatment was added.

Immunocytochemistry

Aptamer-biotin-SAv-C1q complex ability to initiate complement fixation on the target cell was tested using a murine anti-human C9 antibody for the MAC pore forming C9 complement protein, coupled with an anti-mouse Cy5 secondary, along with a Hoechst nuclear stain. An anti-CD59 antibody was also included in two treatment groups, as the anti-CD59 Ab has been shown to inhibit the action of the mCRP CD59. C9 presence on the surface of the target cell indicates that complement has been successfully activated and fixed on the target cell membrane.

After treatment (see Table 2 for treatment summary) and ICC preparation, images were obtained via LSCM. All MCF7 groups showed labeling of some kind, while the MEAR groups showed no C9 labeling; only the Hoechst stain. Multiple ROIs were chosen from each group, drawn by the ImageJ software (see Figure 7 for how this was done), and average pixel intensity values for each ROI were calculated.

Statistical analysis was performed by comparison among the experimental group (Dish 1 – see Table 2), the complement control group (Dish 4), and the negative control (Dish 3) using the AnalystSoft StatsPlus software (www.analystsoft.com). One-way ANOVA with the post-hoc Tukey-Kramer test revealed significant differences among all three groups ($p < 0.0001$, Figure 7).

Table 2. Immunocytochemistry Treatment Summary

Dish	Treatment 1 - 5 min.	Treatment 2 – 10 min.	Treatment 3 – 3 hr.
1	250 µl 5'-biotin-aptamer	200 µl SAv-C1q	200 µl HSCP
2	250 µl 5'-biotin-aptamer	200 µl SAv-C1q	200 µl HSCP + 200 µl anti-CD59
3	250 µl binding buffer	200 µl binding buffer	200 µl binding buffer
4	250 µl binding buffer	200 µl binding buffer	200 µl HSCP
5	250 µl binding buffer	200 µl binding buffer	200 µl HSCP + 200 µl anti-CD59

The effect of addition of the anti-CD59 on anti-C9 labeling was examined. The expected increase in anti-C9 labeling was observed in the experimental (Dish 2). Unexpectedly, the cells in the control (Dish 5) also showed a significant increase in anti-C9 labeling. The increased labeling in both cases was statistically significantly different when compared to any of the other treatments, but not when compared to each other. Raw data can be reviewed in Appendix D.

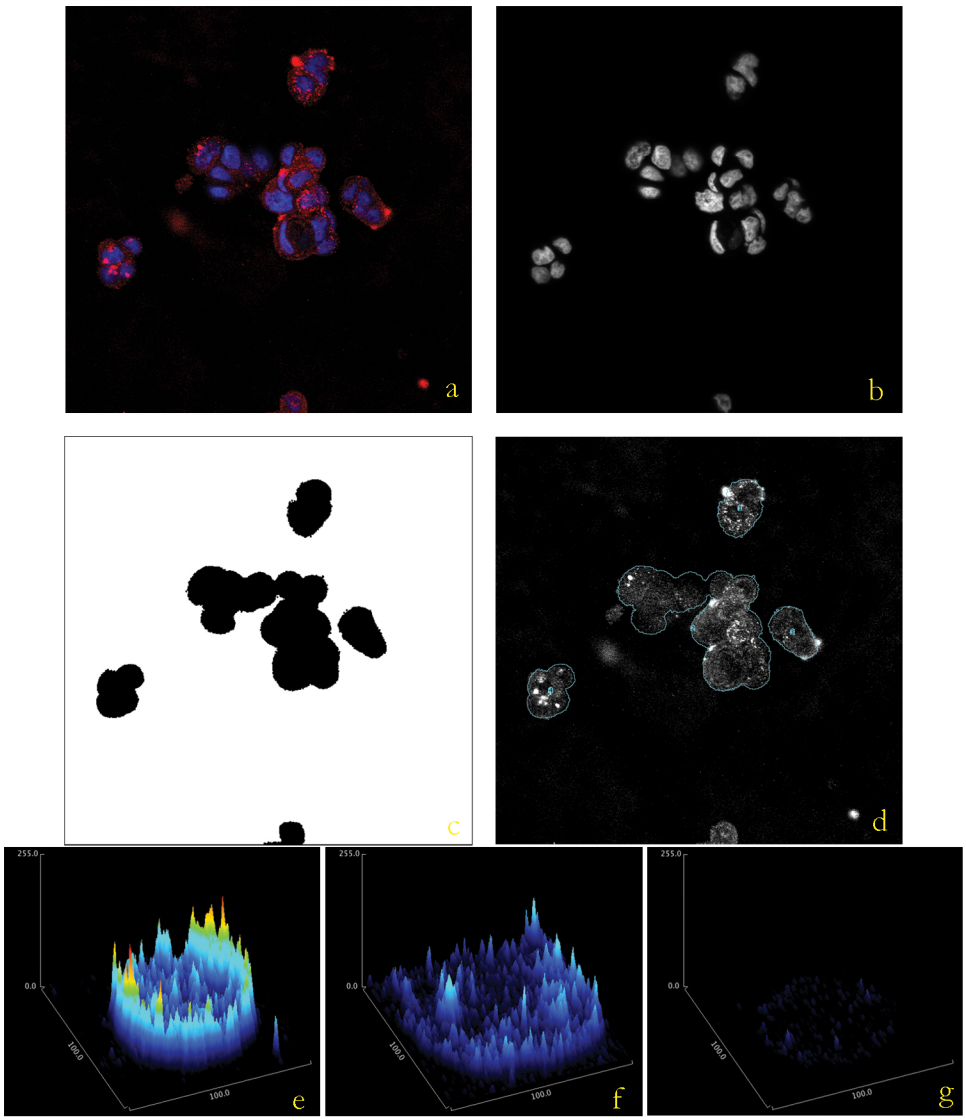

Figure 7. ImageJ Analysis Examples. Image *(a)* shows an image from dish 1, an experimental group. In image *(b)*, the RGB color channels have been split, and the blue channel, representing the nuclei, has been isolated. In *(c)*, the nuclei have been used to create potential regions of interest (ROIs). The ROIs have been overlaid on the isolated red channel in *(d)*, representing anti-C9 Cy5 labeling. Images *(e), (f), and (g)* show pixel intensity heat maps of typical isolated cells from the dish 1 experimental, dish 4 complement control, and dish 3 negative control. Scales on the three images are identical; x and y axes represent physical space on the slide while the z axes represents a grey-scale pixel intensity value from 0 (dark blue/black) to 255 (red).

FRET Analysis

MAC complex formation causes a complete loss of membrane integrity in the targeted cell, eventually leading to lysis and death. Compromising the membrane with MAC lesions may also result in depolarization of the membrane potential voltage of the affected cell prior to lysis and death. As a way to measure this change, two voltage sensitive probes that undergo FRET with each other were loaded into the MCF7 cells. The donor molecule, CC2-DMPE, was excited with a 405 nm laser and emits maximally around 465 nm. 465 nm is in the excitation range of the acceptor molecule $DiSBAC_2(3)$, which emits maximally around 580 nm, allowing them to work as a donor-acceptor pair.

In polarized conditions, these two molecules will be on the same side of the cell membrane, bringing them within the needed Förester distance for FRET to take place, meaning that the acceptor molecule is quenching the donor molecule, and fluoresces strongly at 580 nm. When the membrane depolarizes due to a MAC-induced loss of membrane integrity, the acceptor molecule responds by moving to the interior portion of the cell membrane. This movement separates the acceptor from the donor for FRET to take place. The response in fluorescence is an increase in the 465 nm emission from the donor and a decrease in the 580 emission from the acceptor.

To determine the FRET response ratio for each group, ImageJ was used to create ROIs around the membranes in pre- and post- treatment images, as seen in Figure 8.b. The red and blue channels were split (Figure 8, *c* and *d*), and total pixel intensity values from all ROIs were summed, and divided by the number of pixels (area) of all ROIs within a single image. This provided an average pixel intensity (API) value per ROI across all isolated membranes. Response ratios were calculated as follows:

$$\text{Emission Ratio}_{pre} = \text{Donor API}_{pre} / \text{Acceptor API}_{pre}$$

$$\text{Emission Ratio}_{post} = \text{Donor API}_{post} / \text{Acceptor API}_{post}$$

$$\text{Response Ratio(RR)} = \text{Emission Ratio}_{post} / \text{Emission Ratio}_{pre}$$

Both the treatment and control groups experienced a loss of FRET due to the addition of complement proteins; $\text{Treatment}_{RR} = 1.28$ and $\text{Control}_{RR} = 1.26$. While there was a slight difference in the Response Ratio between the two groups, it is not significant.

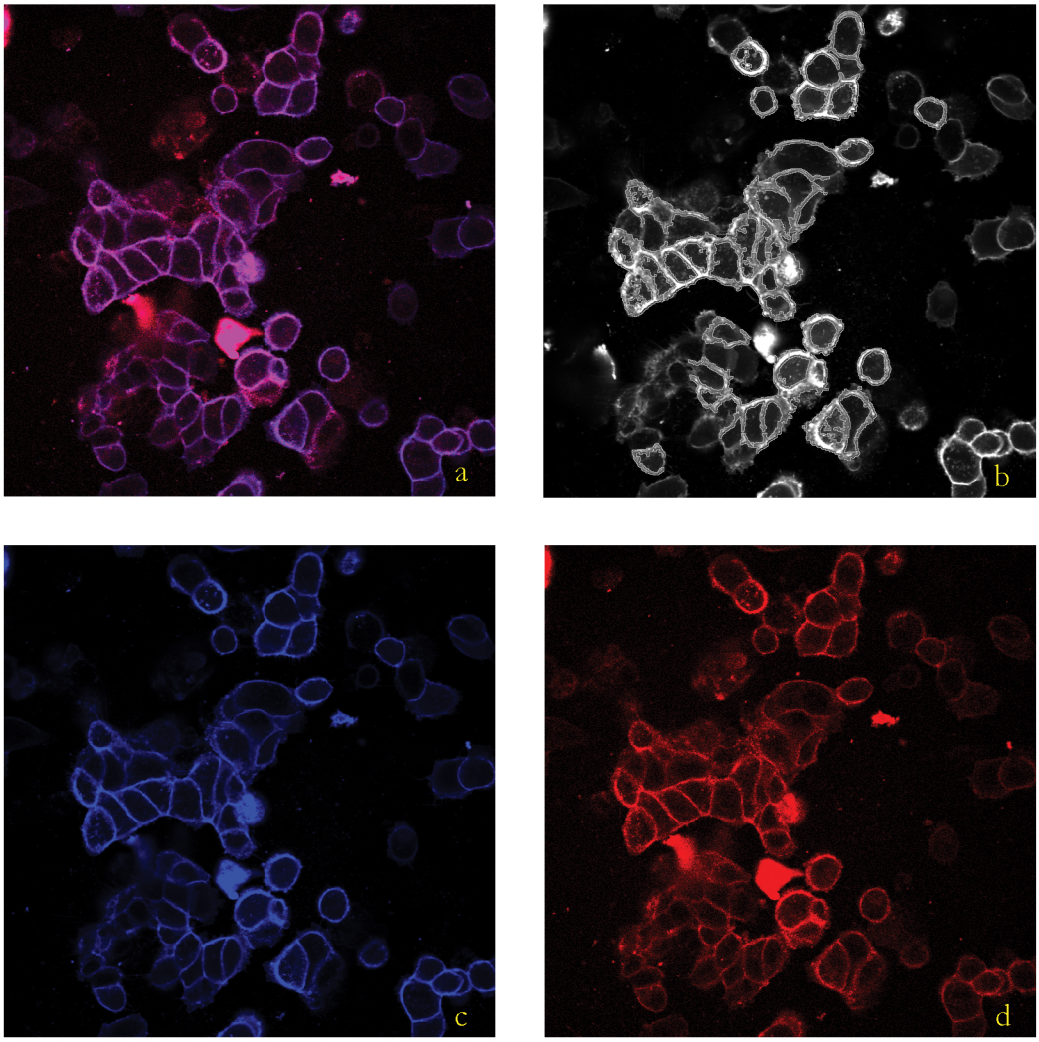

Figure 8. FRET Analysis of MCF7 Cells. Figure *(a)* is a representative image of the MCF7 cells analyzed for FRET in response to treatment. Figure *(b)* shows the ROIs used to generate pixel intensity of the donor *(c)* and acceptor *(d)* channels.

Transmission Electron Microscopy

Two categorical variables were collected for each cell. Each cell was classified as either swollen (representative of potential osmotic lysis) or not swollen and additionally classified as having small breaks in the plasma membrane (potential MACs) or no breaks in the plasma membrane. The first analysis was to determine if there was an association between these two variables within each group: full treatment, HSCP only control, and negative control. A hand calculated comparison of proportions was done for each group, comparing the proportion of all swollen cells that contained membrane breaks to the proportion of all normal cells that contained breaks. See Figure 9 for example and results below.

	Swollen	**Not Swollen**
Membrane Breaks	a	b
No Membrane Breaks	c	d

$$Difference\ in\ Proportions = \left(\frac{a}{a+c}\right) - \left(\frac{b}{b+d}\right)$$

Group	**Difference in Proportions**
Full Treatment (Aptamer-biotin-SAv-C1q)	0.77
HSCP only	0.74
Negative Control	0.67

Figure 9. Differences in Proportions Amongst Groups in TEM Study. The top table shows an example of the 2x2 contingency table used for calculations, with the equation below. The bottom table shows difference in proportions for each group. Values closer to 1 indicate higher degrees of association.

A Fisher's Exact Test was also used to analyze the significance of the association between swollen cells and membrane breaks, and only the full treatment group was found to have significantly associated variables ($p < 0.005$). An overall comparison of all the cells from each group using a Fisher's Exact Test was also used and the degree of association between swollen cells and membrane breaks was also found to be significant, $p < 0.0001$.

The proportions of swollen cells between groups was tested for significant differences using the R Test of Equal or Given Proportions. The full treatment group had significantly more swollen cells than the HSCP control group ($p < 0.05$) and significantly more than the negative control ($p < 0.01$). As expected, there was no significant difference between the HSCP group and negative control ($p > 0.1$). See Figure 10 for data and results.

Sample	Swollen	Non-Swollen	Proportion
EXP	7	13	0.35
HSCP	2	18	0.10
CNTR	1	19	0.05

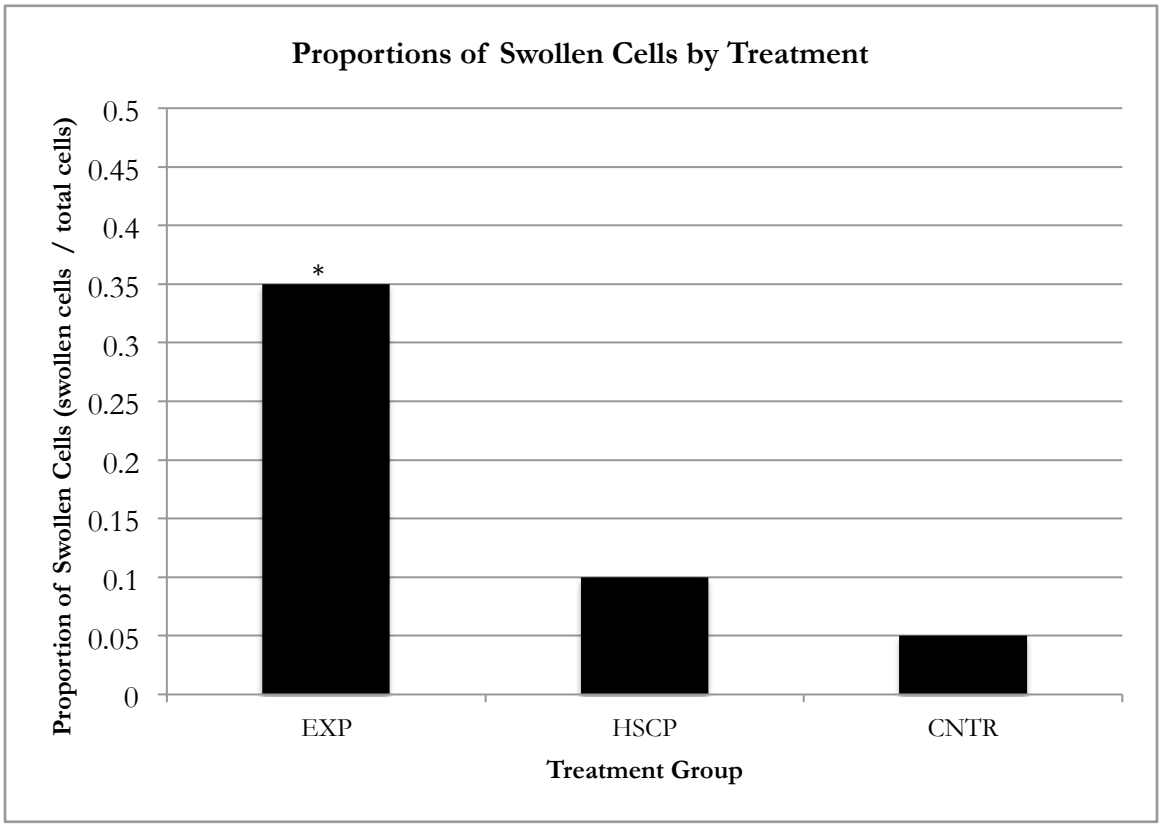

Figure 10. Proportion of Swollen Cells by Treatment in TEM Study. The top table shows counts of swollen and non-swollen cells for the treatment group (EXP – 250 µl Apt-biotin, 200 µl SAv-C1q, 200 µl HSCP), the HSCP only control (HSCP – 450 µl binding buffer, 200 µl HSCP), and the negative control (CNTR – 650 µl binding buffer). The bar graph charts proportions of swollen cells by group. The * indicates the significant difference of EXP from HSCP ($p < 0.05$) and CNTR ($p < 0.01$).

Aptamer Internalization

The localization of the TLS-11a aptamer, in response to temperature, was tested following a chance observation of an aptamer-AF546 treated MEAR culture that had spent the night incubating at 37°C. Upon imaging a second time, the aptamer appeared to have moved into the cell itself. To investigate this further, MEAR cells were cultured on glass coverslips and transferred to the heated stage dishes to keep the culture at approximately 37°C while continuously imaging over a 45 minute to 1 hour period.

Imaging began after a 10 minute waiting period to allow the cells and stage to reach 37°C. AF546 labeled TLS-11a aptamer was added at approximately 2 minutes 30 seconds into imaging. As seen in Figure 11.*b*, strong fluorescent labeling appeared on the membrane of the cell. After approximately 20 minutes, the fluorescent label had migrated internally, as seen in Figure 11.*c*. Temperature dependence of internalization was demonstrated by repeating this experiment at 25°C. Little to no aptamer migration was visible after 25 minutes of imaging. See before and after images in Figure 11, *d* and *f*.

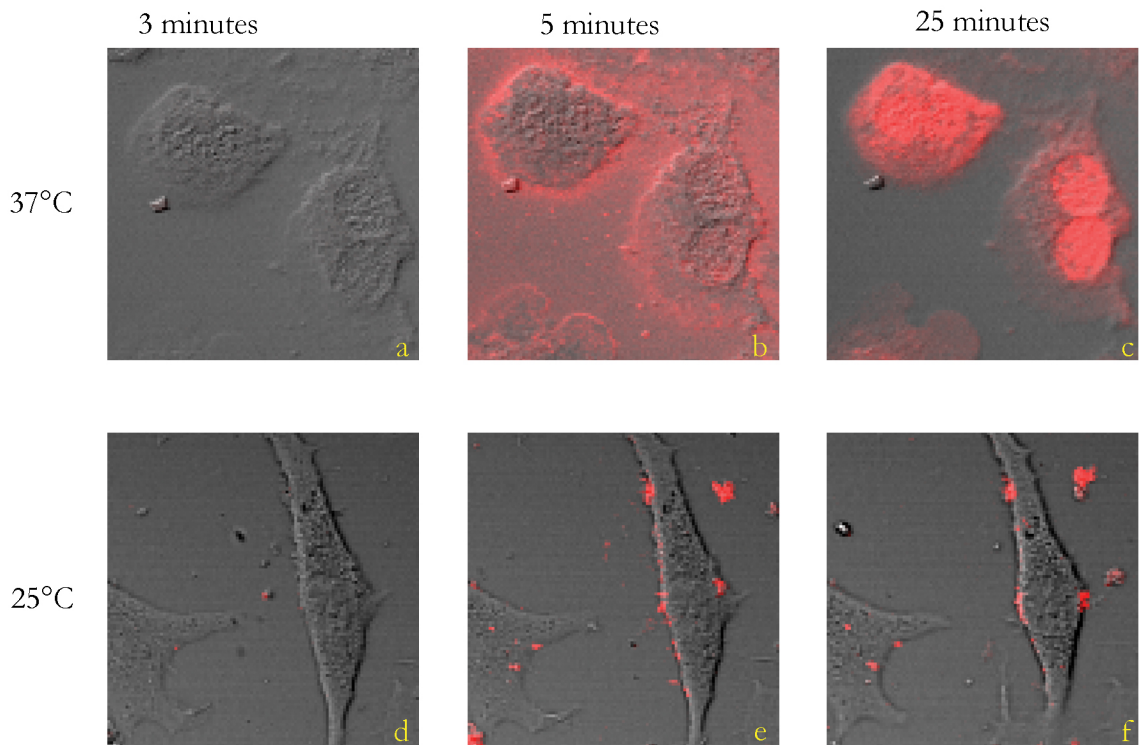

Figure 11. Affect of Temperature on Aptamer Internalization in MEAR cells. The top row of LSCM images show the AF546 modified TLS-11a aptamer migration in MEAR cells at 37°C at 3 minutes *(a)*, 5 minutes *(b)*, and 25 minutes *(c)* after treatment. The bottom row of images show this same treatment at 25°C at 3 minutes *(d)*, 5 minutes *(e)*, and 25 minutes *(f)* after treatment.

CHAPTER 4: DISCUSSION

Overview

The primary hypothesis is that an aptamer-biotin-SAv-C1q complex is capable of initiating the classical complement pathway resulting in MAC formation and cell lysis. The TLS-11a and MUC1-5TR aptamers were found to bind specifically to their target cells (Figure 5), the aptamer and the SAv-C1q complex were found to be bound within 5 and 10 minutes respectively (Figure 6), and an immunocytochemistry study, coupled with quantitative image analysis, found significant C9 deposition on MCF7 cells in response to treatment (Figure 7). The anti-CD59 Ab was found to dramatically increase C9 deposition over groups without anti-CD59 Ab in the their treatment, but no significant difference was found between the two groups with anti-CD50 Ab. FRET analysis showed membrane depolarization in response to complement, but no difference between the treatment and control could be determined (Figure 8). TEM analysis of MCF7 cells found statistically significant increases in swollen cells in the treatment groups, as well as an association between the swollen cells and observed membrane breaks (Figures 9 and 10). The MEAR cell line was similarly investigated using the TLS-11a aptamer, which bound to the cell surface with similar rapidity. However, the MEAR cell line was found to rapidly internalize the TLS-11a aptamer, clearing it from the cell surface within 20 minutes when at 37°C (Figure 10). Preliminary work investigating the destination of the internalized aptamer is underway (Appendix A).

TLS-11a Aptamer Internalization by MEAR Cells

The temperature dependence of internalization of the TLS-11a aptamer by MEAR cells strongly suggests binding of the aptamer to its target triggers receptor-mediated endocytosis. It is possible that the aptamer could adopt different secondary-tertiary structure at 25°C and 37°C, however the similarity between the predicted 2° conformational structures of the TLS-11a aptamer at different temperatures (Figure 4) suggests this is unlikely. As an additional control, the migration of the MUC1-5′TR aptamer was tested at both temperatures on the MCF7 cells. As this aptamer binds to MUC1, a surface-associated protein that is typically shed, not internalized, the AF546 florescence should not spread to the cytoplasm. As expected, no internalization was observed (results not shown).

Further research is needed to analyze the actual cell-surface target to which the TLS-11a aptamer is binding. The rate of internalization suggests a receptor-mediated pathway which typically works via clathrin-coated pits that invaginate clustered receptor-ligand complexes (Goldstein et al., 1985), which has been shown to internalize other aptamers with different cell lines (Li et al., 2011). The binding of a ligand to the receptor can trigger the receptor to migrate and cluster with other ligand-bound receptors in the clathrin-coated pit. Alternatively, some receptors are continuously internalized and returned to the surface via these pits, regardless of the presence of a ligand or not. As reviewed by Goldstein, the internalized vesicle then fuses with early endosomes present just below the surface of the cell. The interior of these early endosomes is slightly acidic, and many ligands will dissociate from their receptor at this point. The receptor typically returns to the surface while the ligand moves on to the appropriate location, determined by some signal sequence. Without a signal sequence directing the ligand elsewhere, the ligand will be moved through

progressively more acidic environments, ending in a lysosome where it will be completely degraded. Some preliminary work has been done on tracking the internalization path using targeted organelle dyes, and can be reviewed in Appendix A.

This result suggests that the TLS-11a aptamer-MEAR cell model will be useful for the study of aptamer based intracellular toxin delivery for cancer cells. Other researchers have had success in using aptamers to deliver photo-toxic substances (Ferreira et al., 2009) and the gelonin toxin (Chu et al., 2006) to the cytosol of cancer cells, inducing cell death.

Complement Fixation: ICC, FRET, and TEM Analysis

As the TLS-11a aptamer was shown to internalize at 37°C within 20 minutes, and this was the temperature for the 3 hour HSCP incubation step during the ICC experiment, it is entirely possible that the aptamer-SAv-C1 complex was internalized before effectively initiating complement fixation. Also curious was the lack of C9 labeling in the two dishes that were treated with the mCRP CD59 inhibiting antibody. The anti-CD59 treatments should, if the MCF7 anti-CD59 dishes are any indication, have dramatically increased the level of C9 deposition. It is possible that the mouse CD59 homolog is different enough in structure that the CD59 antibody was unable to recognize it, but numerous CD59 homologs have been characterized, including the mouse (Qian et al., 2000), and have been shown to be viable models to study human mCRP interactions.

In the MCF7 cell model, the ability of the aptamer-SAv-C1 complex to increase C9 labeling over complement control is significant. This suggests that MAC formation is taking place in response to the aptamer-SAv-C1 treatment as C9 complement proteins are the pore-

forming subunits of the MAC. Of interest is that the pattern of labeling outlined the cells, which was expected. ROIs generally included multiple cells that have divided from each other, meaning their membranes are adjacent. The images suggest this does not have an impact on the ability of complement proteins to penetrate this region, and previous research has shown that both C1 (460 kD) and the anti-CD59 Ab are able to penetrate multiple cell layers into microtumors within just 2 hours (Hakulinen and Meri, 1998). Further, the analyzed images were comprised of multiple images taken at intervals along the z-axis, creating a z-stack. This allows for a much larger portion of the cellular membrane, including the "top" of cells, to be taken into account.

The interaction of the mCRP CD59 inhibiting antibody was dramatic. As shown, treatment with this antibody can be sufficient to allow complement fixation to progress unchecked, which corroborates previous research (Hakulinen and Meri, 1998). It is possible that lower concentrations of the anti-CD59 Ab could augment the effect of the aptamer-SAv-C1 treatment while not completely removing the inhibitory effect of CD59. The anti-CD59 Ab used was an IgG, which itself is fully capable of binding C1 and initiating the classical complement pathway. Cleavage of the IgG and removing the Fc region will allow isolation of the portion that binds and inhibits CD59. This could then be used to inhibit CD59 activity while not initiating the complement pathway, negating any additional activation the IgG may have added. For more detail on this process, see Appendix B. Additionally, there are a number of other mCRPs that should be investigated as inhibition of any of these may help augment the effect as well.

Previous studies using FRET to analyze cell viability make use of the changes in internal chemistry of a cell undergoing apoptosis. Two fluorescent proteins linked by a short

peptide with a caspace-3 cleavage sequence have been used to detect dying cells, as caspace-3 is activated during apoptosis (Loos et al., 2011, Koike-Kuroda et al., 2010, Tyas et al., 2000). Utilizing probes that change their membrane partitioning in response to voltage changes, and experience FRET when sharing the same side of the membrane, have also been used as a fluorescence based approach to monitoring membrane potential changes (Bradley et al. 2009). Using the voltage sensitive probes CC2-DMPE and $DiSBAC_2(3)$ to detect possible membrane potential changes in response to MAC formation is a novel use of these probes. Further refinement of this method may provide a high resolution, real time system for monitoring the effects of MAC formation on the cellular membrane.

The swollen cell morphology seen in the TEM images is expected, as MAC formation does cause osmotic lysis of the cells. That the proportion of swollen cells in the treatment group is significantly larger than the proportion of swollen cells in either control group is important. Of interest is that the proportion of swollen cells in the experimental is 35%, which is very close to the maximum kill rate achieved in a previous study (Bruno, 2010). That the membrane breaks do have a significant association with swollen cells suggests that these breaks are in fact MACs. An immunogold study is currently underway to help clarify this.

Conclusions

Research into the use of aptamers as surrogates of antibodies for diagnostic and therapeutic applications has expanded greatly in the past decade. The advantages aptamers have over antibodies include lack of immunogenicity and much less expensive production costs, particularly after initial development. The SELEX process is flexible enough to allow for selection of ligands under various conditions, whereas antibodies can only be developed

in physiological conditions (Nimjee et al., 2005). Once selected, the continued production does not require the use of cell culture, instead using chemical synthesis with almost no variation between batches (Jayasena, 1999). This chemical synthesis also allows for great flexibility in the types of modifications that can be made to the aptamer, some of which have been shown in this study.

In this study, I explored two different aptamers and their ability to bind to and initiate complement-based destruction of two different cancer cell lines. In the murine liver cancer cell line, BNL 1ME A.7R.1 (MEAR), the TLS-11a aptamer was quickly internalized at physiological temperatures and was completely ineffective at initiating the complement pathway. However, the TLS-11a aptamer is therefore a potential candidate for intracellular toxin delivery as a means of inducing targeted apoptosis of the MEAR cancer cells. In the human breast cancer cell line MCF7, the biotinylated MUC1-5TR aptamer via a streptavidin-C1q conjugation was shown by immunofluorescence, FRET analysis, and TEM imaging to rapidly initiate the classical complement pathway leading to MAC formation and destruction of the target cell. These results provide further evidence that aptamer therapy can provide a non-toxic, non-immunogenic, relatively inexpensive, specific form of chemotherapy.

Appendix A – TLS-11a Aptamer Localization

The CellLight® BacMam 2.0 (Invitrogen) system was used in an attempt to fluorescently label specific intracellular organelles, thus allowing identification by colocalization of the TLS-11a aptamer-SAv-AF546 fluorescence. This system takes advantage of an insect baculovirus, which has been transfected with human promoters associated with genes that express fluorescent proteins attached to specific organelle targeting sequences, with the intent of causing delivery of the fluorescent gene products (proteins) to specific locations in the cell (Kost et al., 2005). As the baculovirus is specific to insects, only the human promoter controlled genes are expressed. While the MEAR cell line is mouse derived, the organelle labels were still expressed in early trials.

As the ribosome begins to translate the mRNA of the transfected gene, a signal-recognition particle (SRP) recognizes a specific peptide sequence and binds to the ribosome to slow down translation. The signal recognition particle then binds to a SRP-receptor on the endoplasmic reticulum (ER), facilitating the ribosome binding to a translocation complex on the membrane of the ER. The signal-recognition particle dissociates and gene translation continues, feeding the new peptide chain into the cisternal space of the ER.

Once translation is complete, the new proteins are glycosylated and packaged into vesicles that have been coated with a special protein marking the vesicle for delivery to the Golgi apparatus. The vesicle fuses with the Golgi apparatus at which point the proteins undergo any additional enzymatic modifications and are sorted into vesicles based

on the destination indicated by their signal sequences. These vesicles bud off from the Golgi apparatus and move on to deliver the proteins to their final destinations.

Four specific protein labels were chosen for this study, each comprised of a fluorescent label and unique targeting sequence; Plasma Membrane – CFP used the Lck tyrosine kinase myristolyation/palmitoylation sequence (Kabouridis et al., 1997), lysosome – GFP used the lysosomal associated membrane protein 1 sequence (Falcón-Pérez et al. 2005), early endosome – GFP used the Rab5a sequence (Mairhofer et al., 2009), and the golgi apparatus – GFP used the Golgi-resident enzyme N-acetylgalactosaminyltransferase 2 (Storrie et al., 1998).

Cell cultures were loaded with 20 µl of $1x10^8$ CellLight® particles/mL reagent solution and returned to the incubator (37°C, humidified 5% CO_2) for 48 hours prior to experimentation and imaging. For more details on the experimental methods, please reference the Aptamer Synthesis and Binding Kinetics section in Chapter 2. Preliminary results can be seen in Figure 12.

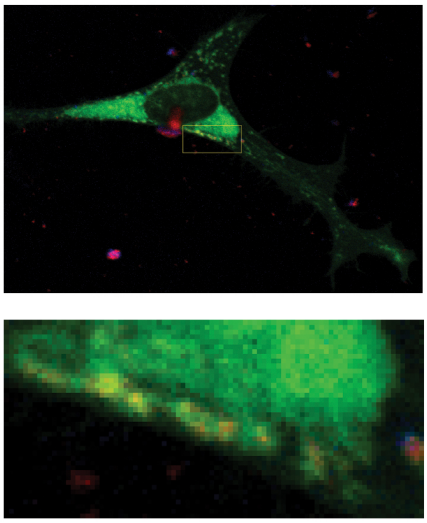

Figure 12. Localization of TLS-11a Aptamer. The top image is of a MEAR cell that had been treated with the Lysosome-GFP label, along with AF-546 labeled TLS-11a aptamer. In the lower image, colocalization of the aptamer with the lysosome is represented by yellow.

Appendix B – Anti-CD59 IgG

The antibody used in this study to inhibit the mCRP CD59 is an immunoglobulin G. IgG and IgM molecules are both capable of activating the classical complement pathway by binding of C1 to the Fc portion of the Ig (Lightle et al., 2009, Kojouharova et al., 2004). Immunoglobulins consist of two heavy chains and two light chains that are held together through multiple disulfide bonds, a strong structural bond between the sulfur atoms of two cysteine residues in the Ig. Cysteine is only one of two amino acids to contain a sulfur atom, and the only one capable of forming these bonds. These bonds are initially formed by oxido-reductases in the endoplasmic reticulum while the Ig is being folded into shape (Inaba and Ito, 2008).

Cleavage of these bonds using a commercially available digestion kit can allow one to isolate the Fc and Fab fragments from each other (Girardi et al., 2009). These kits make use of papain, a cysteine-endopeptidase that breaks the disulfide bond holding the Ig together. By isolating the Fab fragment, the fragment that actually binds to CD59, the mCRP CD59 can be inhibited without the Fc portion of the IgG binding C1 and activating the classical complement pathway. This will allow for better characterization of the regulatory effect CD59 has on MAC formation.

Appendix C – Binding Kinetics Data

MEAR

Aptamer Binding

ROI		AREA	MEAN	StdDev	IntDen	Seconds	ROI 1	ROI 2	ROI 3
0:7.02.859	1	4971	41.635	42.792	206968	422.859	41.635	59.864	33.551
	2	552	59.864	59.472	33045	391.547	39.297	61.217	31.882
	3	1683	33.551	28.024	56466	360.219	35.849	53.12	28.677
						328.891	31.995	47.478	24.551
0:6.31.547	4	4971	39.297	42.857	195346	302.797	27.258	39.62	21.332
	5	552	61.217	58.075	33792	287.141	25.724	39.984	19.574
	6	1683	31.882	28.664	53658	271.469	25.096	40.185	19.214
						255.813	28.323	43.223	23.898
0:6.00.219	7	4971	35.849	41.475	178204	240.141	29.826	45.815	25.266
	8	552	53.12	52.09	29322	224.484	28.85	40.386	24.289
	9	1683	28.677	27.1	48264	208.813	23.756	32.685	20.264
						193.156	13.15	18.484	10.062
0:5.28.891	10	4971	31.995	38.831	159046	182.703	1.91	4.071	1.49
	11	552	47.478	47.627	26208	151.391	0.004	0.049	0
	12	1683	24.551	26.321	41319	120.078	0.000	0	0
						93.969	0.000	0	0
0:5.02.797	13	4971	27.258	37.512	135499	62.656	0.000	0.098	0
	14	552	39.62	45.623	21870	31.328	0.000	0	0
	15	1683	21.332	26.274	35901	0.000	0.000	0	0
0:4.47.141	16	4971	25.724	37.862	127875				
	17	552	39.984	45.961	22071				
	18	1683	19.574	27.047	32943				
0:4.31.469	19	4971	25.096	36.18	124752				
	20	552	40.185	44.602	22182				
	21	1683	19.214	26.01	32337				
.									
.									
.									
0:0.31.328	52	4971	0.004	0.085	18				
	53	552	0	0	0				
	54	1683	0	0	0				
0:0.00.000	55	4971	0	0	0				
	56	552	0	0	0				
	57	1683	0	0	0				

Appendix D - ICC Raw Data

ImageJ ROI Measurements

TREATMENT

	ROI		Area	Mean	StdDev	IntDen
		1	6937	57.992	59.336	402289
		2	38955	44.713	48.646	1741788
		3	6016	41.929	41.389	252243
		4	7133	51.277	58.3	365758
		5	25656	54.694	50.394	1403223
		6	52004	41.938	38.65	2180925
		7	62959	49.612	41.036	3123516
		8	38084	38.504	38.476	1466377
		9	4025	39.696	36.402	159776
TOTALS	**45**		**241769**	**420.355**	**412.629**	**11095895**

HSCP

	ROI		Area	Mean	StdDev	IntDen
		1	28412	13.605	22.455	386553
		2	10084	10.551	15.589	106400
		3	121313	24.897	28.942	3020368
		4	45406	31.181	47.48	1415810
		5	44566	28.524	42.02	1271221
		6	70490	20.765	28.094	1463740
TOTALS	**21**		**320271**	**129.523**	**184.58**	**7664092**

CONTROL

	ROI		Area	Mean	StdDev	IntDen
		1	6045	0.586	3.856	3541
		2	5710	2.189	7.142	12499
		3	4698	0.18	1.734	845
		4	3653	1.573	6.14	5746
		5	15203	0.881	4.22	13395
		6	17449	0.468	2.909	8160
		7	85371	3.201	10.958	273287
		8	5759	2.697	9.8	15530
		9	15523	3.419	11.117	53074
TOTALS	**45**		**159411**	**15.194**	**57.876**	**386077**

ANOVA Analysis

Observation (ROI)	Treatment	HSCP	Control
1	57.992	13.605	0.586
2	44.713	10.551	2.189
3	41.929	24.897	0.18
4	51.277	31.181	1.573
5	54.694	28.524	0.881
6	41.938	20.765	0.468
7	49.612		3.201
8	38.504		2.697
9	39.696		3.419

Analysis of Variance (One-Way)

Summary

Groups	*Sample size*	*Sum*	*Mean*	*Variance*
Treatment	9.0000	420.3550	46.7061	20019.6100
HSCP	6.0000	129.5230	21.5872	3133.3390
Control	9.0000	15.1940	1.6882	37.8468
Total	24.0000	*0*	23.5447	429.8418

ANOVA

Source of Variation	*d.f.*	*SS*	*MS*	*F*	*p-level*	*F crit*	*Omega Sqr.*
Between Groups	2.0000	9150.4010	4575.2000	130.5496	0.0000	3.4668	0.9152
Within Groups	21.0000	735.9595	35.0457				
Total	23.0000	9886.3600					

Hartley Fmax	44.2513	*Degrees Of F*	3.0000	8.0000	
Cochran C	0.5751	*Degrees Of F*	3.0000	8.0000	
Bartlett Chi-square	18.0322	*Degrees Of F*	2.0000	*p-level*	0.0001

Comparisons among groups (Factor 1 - Factor #1)

Scheffe contrasts among pairs of means

Group vs Group	*Difference*	*Test Statistic*	*sitical Value(5*	*Accepted?*
1 vs 2	25.1189	8.0507	2.6162	*accepted*
1 vs 3	45.0179	16.1315	2.6162	*accepted*
2 vs 3	19.8989	6.3777	2.6162	*accepted*

Tukey-Kramer Test for Differences Between Means

Groups	*Difference*	*Test Statistics*	*p-level*	*Accepted?*
1 vs 2	25.1189	11.3855	0.0000	*accepted*
1 vs 3	45.0179	22.8134	0.0000	*accepted*
2 vs 3	19.8989	9.0194	0.0000	*accepted*

Bonferroni Test for Differences Between Means

Alpha/N 0.0167

Groups	*Difference*	*Test Statistics*	*p-level*	*Accepted?*
1 vs 2	25.1189	6.3874	0.0000	*accepted*
1 vs 3	45.0179	19.1317	0.0000	*accepted*
2 vs 3	19.8989	7.2816	0.0000	*accepted*

Fisher LSD

Group vs Group	*Difference*	*Test Statistics*	*p-level*	*Accepted?*
1 vs 2	25.1189	8.0507	0.0000	*accepted*
1 vs 3	45.0179	16.1315	0.0000	*accepted*
2 vs 3	19.8989	6.3777	0.0000	*accepted*

Appendix E – FRET Data

Raw Data

D1

PRE 1

Donor (blue)	area	mean	StdDev	IntDen
1	86906	63.469	47.013	5515853
2	603	36.443	11.506	21975
3	1009	47.074	29.91	47498
4	433	28.441	14.586	12315
5	656	43.739	39.994	28693
6	426	18.143	6.6	7729
7	1931	56.616	53.878	109325
8	1126	39.762	51.565	44772
9	338	36.861	4.951	12459
10	4600	36.282	37.641	166895
11	7167	56.485	53.521	404831
12	2341	16.037	38.041	37543
Acceptor (red)				
13	86906	53.769	41.279	4672848
14	603	36.914	21.015	22259
15	1009	37.788	26.665	38128
16	433	23.758	17.435	10287
17	656	33.427	29.651	21928
18	426	24.967	17.528	10636
19	1931	54.746	51.132	105715
20	1126	28.702	33.074	32318
21	338	28.027	15.904	9473
22	4600	40.822	39.505	187783
23	7167	40.883	38.549	293012
24	2341	22.072	32.727	51670

POST

Donor (blue)				
1	86906	65.894	45.57	5726625
2	603	49.367	14.264	29768
3	1009	30.579	9.789	30854
4	433	15.376	12.596	6658
5	656	26.564	18.998	17426
6	426	17.026	14.001	7253
7	1931	57.468	42.532	110970
8	1126	29.576	39.953	33303
9	338	23	4.369	7774
10	4600	44.311	30.04	203832
11	7167	52.091	38.526	373339
12	2341	23.619	26.575	55293
Acceptor (Red)				
13	86906	44.304	36.647	3850293
14	603	34.086	20.413	20554
15	1009	20.344	15.786	20527
16	433	11.231	12.84	4863
17	656	15.181	15.167	9959
18	426	15.216	13.593	6482
19	1931	34.596	30.619	66804
20	1126	16.555	19.817	18641
21	338	13.624	11.59	4605
22	4600	27.117	23.185	124740
23	7167	31.08	26.723	222751
24	2341	16.802	20.026	39334

D2

PRE 1

Donor (blue)	area	mean	StdDev	IntDen
1	5086	129.78	60.616	660059
2	1616	148.612	73.977	240157
3	728	102.952	42.555	74949
4	781	102.389	42.906	79966
5	1710	116.025	54.113	198402
6	19839	134.299	57.139	2664353
7	2946	107.357	47.633	316274
8	1160	103.421	29.191	119968
9	10379	131.533	57.483	1365181
10	1161	106.922	34.485	124136
11	1085	125.92	60.197	136623
12	4451	128.426	56.933	571624
13	783	99.323	36.181	77770
Acceptor (red)				
14	5086	107.225	58.799	545348
15	1616	152.116	74.384	245820
16	728	104.078	51.73	75769
17	781	77.798	40.751	60760
18	1710	95.861	52.138	163922
19	19839	122.969	58.765	2439580
20	2946	104.483	53.176	307808
21	1160	92.716	40.253	107551
22	10379	117.376	63.135	1218244
23	1161	94.015	43.063	109151
24	1085	89.32	51.291	96912
25	4451	91.357	48.958	406632
26	783	84.356	43.262	66051

POST 2

Donor (blue)				
1	5086	100.996	62.631	513667
2	1616	104.929	85.335	169566
3	728	43.036	40.629	31330
4	781	66.344	42.468	51815
5	1710	69.942	39.621	119600
6	19839	101.271	56.916	2009123
7	2946	67.185	42.795	197927
8	1160	53.39	26.191	61932
9	10379	108.78	61.218	1129024
10	1161	87.267	26.135	101317
11	1085	74.617	56.564	80959
12	4451	113.014	60.891	503027
13	783	43.955	42.234	34417
Acceptor (Red)				
14	5086	73.737	52.377	375027
15	1616	90.78	76.244	146701
16	728	38.049	34.447	27700
17	781	39.65	30.538	30967
18	1710	49.774	33.534	85114
19	19839	84.649	52.198	1679359
20	2946	60.689	42.288	178791
21	1160	44.74	29.218	51898
22	10379	83.392	55.723	865528
23	1161	68.725	34.772	79790
24	1085	49.965	39.477	54212
25	4451	72.458	43.52	322509
26	783	33.351	34.717	26114

Response Ratio Calculations

DISH 1

6409888	blue(pre) int total
107536	blue(pre) area total
6603095	blue(post) int total
107536	blue(post) area total
5456057	red(pre) int total
107536	red(pre) area total
4389553	red(post) int total
107536	red(post) area total

59.60690373	blue(pre)
61.40357648	blue(post)
50.7370276	red(pre)
40.81938142	red(post)

1.174820571	Emission Ratio(pre) = blue(pre) / red(pre)
1.504275037	Emission Ratio(post) = blue(post) / red(post)
1.280429602	**Response Ratio = Emission Ratio(post) / Emission Ratio(pre)**

DISH 2

6629462	blue(pre) int total
51725	blue(pre) area total
5003704	blue(post) int total
51725	blue(post) area total
5843548	red(pre) int total
51725	red(pre) area total
3923710	red(post) int total
51725	red(post) area total

128.1674625	blue(pre)
96.73666506	blue(post)
112.9733784	red(pre)
75.85712905	red(post)

1.134492606	Emission Ratio(pre) = blue(pre) / red(pre)
1.275248171	Emission Ratio(post) = blue(post) / red(post)
1.124069178	**Response Ratio = Emission Ratio(post) / Emission Ratio(pre)**

REFERENCES

Berdeaux, G.H., Nordmann, J.P., Colin, E., Arnould, B. *Vision-related Quality of Life in Patients Suffering From Age-related Macular Degeneration.* Am J of Opthalmol (2005) 139:271-279

Bradley, J., Luo, R., Otis, T.S., DiGregorio, D.A. *Submillisecond Optical Reporting of Membrane Potential In Situ Using a Neuronal Tracer Dye.* Jour of Neurosci (2009) 29(29)9197-9209

Bruno, J.G., Carrillo, M.P., Phillips, T., *In Vitro Antibacterial Effects of Antilipopolysaccharide DNA Aptamer-C1qrs Complexes*. Folia Microbiol (2008) 4:295-302

Bruno, J.G. *Aptamer-biotin-streptavidin-C1q complexes can trigger the classical complement pathway to kill cancer cells.* In Vitro Cell Dev Biol (2010) 46(2):107-113

Cao, Z., Tong, R., Mishra, A., Xu, W., Wong, G.C.L., Cheng, J., Lu, Y. *Reversible Cell-Specific Drug Delivery with Aptamer-Functionalized Lipsomes.* Angew Chem Int Ed (2009) 48:6494-6498

Chu, T.C, Marks III, J.W., Lavery, L.A., Faulkner, S., Rosenblum, M.G., Ellington, A.D., Levy, M. *Aptamer:Toxin Conjugates that Specifically Target Prostate Tumor Cells*. Cancer Research (2006) 66(12)5989-5992

Dhar, S., Gu, F.X., Langer, R., Farokhzad, O.C., Lippard, S.J. *Targeted delivery of cisplatin to prostate cancer cells by aptamer functionalized Pt(IV) prodrug-PLGA-PEG nanoparticles.* Proceedings of the National Academy of Sciences (2008) 105(45)17356-17361

Ellington, A.D., Szostak, J.W. *In vitro selection of RNA molecules that bind specific ligands.* Nature (1990) 346:818-822

Falcón-Pérez, J.M., Nazarlan, R., Sabatti, C., Dell'Angelica, E.C. *Distribution and dynamics of Lamp1-containing endocytic organelles in fibroblasts deficient in BLOC-3*. Jour Cell Sci (2005) 118:5243-5255

Ferreira, C.S.M., Matthews, C.S., Missailidis, S. *DNA Aptamers That Bind to MUC1 Tumor Marker: Design and Characterization of MUC1-Binding Single-Stranded DNA Aptamers*. Tumor Biol (2006) 27:289-301

Ferreira, C.S.M., Papamichael, K., Guilbalt, G., Schwarzacher, Gariepy, J., Missailidis, S. *DNA aptamers against the MUC1 tumor marker: design of aptamer-antibody sandwhich ELISA for the early diagnosis of epithelial tumours.* Anal Bioanal Chem (2008) 390(4):1039-1050

Ferreira, C.S.M., Cheung, M.C., Missailidis, S., Bisland, S., Gariépy, J. *Phototoxic aptamers selectively enter and kill epithelial cancer cells.* Nucleic Acids Research (2009) 37(3):866-876

Fishelson, Z., Donin, N., Zell, S., Schultz, S., Kirschfink, M. *Obstacles to cancer immunotherapy: expression of membrane complement regulatory proteins (mCRPs) in tumors.* Molecular Immunology (2003) 40:109-123

Girardi, E., Holdom, M.D., Davies, A.M., Sutton, B.J., Beavil, A.J. *The crystal structure of rabbit IgG-Fc.* Biochem J (2009) 417:77-83

Goldstein, J.L., Brown, M.S., Anderson, R.G.W., Russell, D.W., Schneider, W.J. *Receptor-Mediated Endocytosis: Concepts Emerging from the LDL Receptor System.* Ann Rev Cell Biol (1985) 1:1-39

Hakulinen, J., Meri, S. *Complement-Mediated Killing of Microtumors in Vitro.* American Journal of Pathology (1998) 153(3):845-855

Hofacker, I.L. *Vienna RNA secondary structure server.* Nucleic Acids Research (2003) 31(13):3429-3431

Hornik, K. *The R FAQ.* http://www.r-project.org/ (2011) ISBN 3-900051-08-9

Huan, J., Moore, J., Soffer, S., Kim, E., Rowe, D., Manley, C.A., O'Toole, K., Middlesworth, W., Stolar, C., Yamashiro, D., Kandel, J. *Highly Specific Antiangiogenic Therapy Is Effective in Suppressing Growth of Experimental Wilms Tumors.* Jour of Pediatric Surgery (2001) 36(2):357-361

Inaba, K., Ito, K. *Structure and mechanisms of the DsbB-DsbA disulfide bond generation machine.* Biochimica et Biophysica Acta (2008) 1783:520-529

Jayasena, S.D. *Aptamers: An Emerging Class of Molecules That Rival Antibodies in Diagnostics.* Clinical Chemistry (1999) 45(9)1628-1650

Jurianz, K., Maslak, S., Garcia-Schüler, H., Fishelson, Z., Kirschfink, M. *Neutralization of complement regulatory proteins augments lysis of breast carcinoma cells targeted with rhumAB anti-HER2.* Immunopharmocology (1999) 42:209-218

Kabouridis, P.S., Magee, A.I., Ley S.C. *S-acylation of LCK protein tyrosine kinase is essential for its signaling function in T lymphocytes.* The EMBO Journal (1997) 16(16)4983-4998

Kojouharova, M.S., Gadjeva, M.G., Tsacheva, I.G., Zlatarova, A., Roumenina, L.T., Tchorbadjieva, M.I., Atanasov, B.P., Waters, P., Urban, B.C., Sim, R.B., Reid, K.B.M., Kishore, U. *Mutational Analyses of the Recombinant Globular Regions of Human C1q A, B, and C Chains Suggest an Essential Role for Arginine and Histidine Residues in the C1q-IgG Interaction*. Jour Immunol (2004) 172:4351-4358

Kost, T.A., Condreay, J.P., Jarvis, D.L. *Baculovirus as versatile vectors for protein expression in insect and mammalian cells.* Nature Biotechnology (2005) 23(5)567-575

Koike-Kuroda, Y., Kakeyama, M., Fujimaki, H., Tsukahara, S. *Use of live imaging analysis for evaluation of cytotoxic chemicals that induce apoptotic cell death.* Toxicology in Vitro (2010) 24:2012-2020

Kwon, O.S., Park S.J., Jang, J. *A high-performance VEGF aptamer functionalized polypyrrole nanotube biosensor.* Biomaterials (2010) 31:4740-4747

Lee, H.S., Kim, K.S., Kim, C.J., Hahn, S.K., Jo, M.H. *Electrical detection of VEGFs for cancer diagnoses using anti-vascular endotherial [sic] growth factor aptamer-modified Si nanowires FETs.* Biosensors and Bioelectronics (2009) 24:1801-1805

Lee, I.H., An, S., Yu, M.K., Kwon, H.K., Im, S.H., Jon, S. *Targeted chemoimmunotherapy using drug-loaded aptamer-dendrimer bioconjugates.* J Control Release (2011) doi: 10.1016/j.jconrel.2011.05.025

Lee, J.H., Vigit, M.V., Mazumdar, D., Lu, Y. *Molecular diagnostic and drug delivery agents based on aptamer-nanomaterial conjugates.* Adv Drug Del Rev (2010) 62:592-605

Li, N., Nguyen, H.H., Byrom, M., Ellington, A.D. *Inhibition of Cell Proliferation by an Anti-EGFR Aptamer.* PLoS ONE (2011) 6(6)e20299, doi:10.1371/journal.pone.0020299

Lightle, S., Aykent, S., Lacher, N., Mitaksov, V., Wells, K., Zobel, J., Oliphant, T. *Mutations within a human IgG2 antibody form distinct and homogeneous disulfide isomers but do not affect Fc gamma receptor or C1q binding.* Protein Science (2010) 19:753-762

Loos, B., Genade, S., Ellis, B., Lochner, A., Engelbrecht, A.M. *At the core of survival: Autophagy delays the onet of both apoptotic and necrotic cell death in a model of ischemic cell injury.* Exp Cell Resear (2011) 317:1437-1453

Osborne, S.E., Matsumura, I., Ellington, A.D. *Aptamers as therapeutic and diagnostic reagents: problems and prospects.* Current Opinion Chem Biol (1997) 1:5-9

Mairhofer, M., Steiner, M., Salzer, U., Prohaska, R. *Stomatin-like Protein-1 Interacts with Stomatin and Is Targeted to Late Endosomes*. Jour Bio Chem (2009) 284(42)29218-29229

Malik, A.K., Gerber, H.P. *Targeting VEGF ligands and receptors in cancer*. Targets (2003) 2(2)48-57

Min, K., Jo, H., Song, K., Cho, M., Chun, Y.S., Jon, S., Kim, W.J., Ban. C. *Dual-aptamer-based delivery vehicle of doxorubicin to both PSMA (+) and PSMA (-) prostate cancers*. Biomaterials (2011) 32:2124-2132

Mukhopadhyay, P., Chakraborty, S., Ponnusamy, M.P., Lakshmanan, I., Jain, M., Batra, S.K. *Mucins in the pathogenesis of breast cancer: Implications in diagnosis, prognosis and therapy*. Biochimica et Biophysica Acta (2011) 1815:224-240

Nimjee, S.M., Rusconi, C.P., Sullenger, B.A. *Aptamers: An Emerging Class of Therapeutics*. Annu Rev Med (2005) 56:555-583

Qian, Y.M., Qin, X., Miwa, T., Sun, X., Halperin, J.A., Song, W.C. *Identification and Functional Characterization of a New Gene Enconding the Mouse Terminal Complement Inhibitor CD59*. Jour of Immunol (2000) 165:2528-2534

Rosse, W.F., Dourmashkin, R., Humphrey, J.H. *Immune Lysis of Normal Human and Paroxysmal Nocturnal Hemoglobinuria (PNH) Red Blood Cells : III. The Membrane Defects Caused by Complement Lysis*. Jour of Exp Med (1966) 123:969-984

Sarraf-Yazdi, S., Mi, J., Moeller, B., Niu, X., White, R.R., Kontos, C.D., Sullenger, B.A., Dewhirst, M.W., Clary, B.M. *Inhibition of In Vivo Angiogenesis and Growth Via Systemic Delivery of an Angiopoietin 2-Specific RNA Aptamer*. Jour of Surgical Research (2008) 146:16-23

Shangguan, D., Meng, L., Cao, Z.C., Xiao, Z., Fang, X., Li, Y., Cardona, D., Witek, R.P., Liu, C., Tan, W. *Identification of Liver Cancer-Specific Aptamers Using Whole Live Cells*. Anal. Chem. (2008) 80:721-728

Storrie, B., White, J., Röttger, S., Stelzer, E.H.K., Suganuma, T., Nilsson, T. *Recycling of Golgi-resident Glycosyltransferases through the ER Reveals a Novel Pathway and Provides an Explanation for Nocodazole-induced Golgi Scattering*. Jour Cell Bio (1998) 143(6)1505-1521

Thorsteinsson, L., O'Dowd, G.M., Harrington, P.M., Johnson, P.M. *The complement regulatory proteins CD46 and CD59, but not CD55, are highly expressed by glandular epithelium of human breast and colorectal tumour tissues*. APMIS (1998) 106:869-878

Tuerk, C., Gold, L. *Systematic Evolution of Ligands by Exponential Enrichment: RNA Ligands to Bacteriophage T4 DNA Polymerase.* Science (1990) 249:505-510

Tyas, L., Brophy, V.A., Pope, A., Rivett, A.J., Tavaré, J.M. *Rapid caspase-3 activation during apoptosis revealed using fluorescence-resonance energy transfer.* EMBO Reports (2000) 1(3)266-270

Wagner, E., Frank, M.M. *Therapeutic potential of complement modulation.* Nature Reviews|Drug Discovery (2010) 9:43-56

Zhou, B., Wang, B. *Pegaptanib for the treatment of age-related macular degeneration.* Exp Eye Research (2006) 83:615-619

American Cancer Society. *Cancer Facts & Figures 2009.* Atlanta:American Cancer Society 2009

National Cancer Institute. *Cancer | Changing the Conversation. The Nation's Investment in Cancer Research – An Annual Plan and Budget Proposal for Fiscal Year 2012.* NIH Publication No. 11-7760 (2011)

The Web site of the National Cancer Institute (http://www.cancer.gov)

VITAE

John Richard Stecker was born in Houston, Texas on April 4th, 1984, the son of James Everett Stecker and Susan Lynn Stecker. After completing his work at Bellaire High School, Bellaire, Texas, in 2002, he entered The University of Texas at San Antonio. After two semesters of work, he transferred to The University of Texas at Austin in 2003. During the summer of 2005, he attended the University of Wurzburg, Wurzburg, Germany. He received the degree of Bachelor of Science with a focus in Neurobiology from UT-Austin in August of 2007. He worked as a Systems Support technician for PeopleAdmin, Inc., Austin, Texas, for the two years following. In the fall of 2009, he entered the Graduate College of Texas State University-San Marcos.

Permanent Email Address: fourstecker@gmail.com

This thesis was typed by John R. Stecker